Abstract

Harb, Hussein Said. A Probabilistic Approach to Damage Localization in Structural Health Monitoring. (Under the direction of Dr. Fuh-Gwo Yuan.)

A probabilistic framework for on-line structural health monitoring of plate-like structures, which addresses the issue of uncertainties inherent in the problem of damage detection, is presented. This work answers the following question in a probabilistic approach:

Based on the available data, and acknowledging the uncertainty inherent in the problem, what is the probability that the damage occurs at a certain location in a structure?

Gaussian probability density functions (PDF) have been used to model the different types of uncertainties. These uncertainties that are presented in this work, include stochastic and model uncertainties. Considering these types of uncertainties, the main objective is to locate the damage in a plate structure in a probabilistic form. Also, the sensitivity of damage localization to the levels of uncertainties is presented in this work.

The probabilistic structural health monitoring employed in this study can be presented in the following steps:

Firstly, an elastic wave energy decay model in relation to the propagation distance for the damage localization problem in isotropic plates is chosen. A Gaussian PDF is used to represent the uncertainty that is due to the underlying assumptions, which simplify the physical model.

Secondly, the uncertain measured sensor data (stochastic uncertainty) is modeled as a Gaussian PDF.

Thirdly, a least-squares damage localization technique is applied to iteratively search for the location of the damage based on elastic wave energy measurements.

To model the PDFs of the stochastic and model uncertainties, and to solve for the resultant PDF of the location of the damage (output) using the PDFs of the measured and modeled data (input), the Monte Carlo method is used.

Lastly, probabilistic diagrams for the damage location can be constructed using the moments (mean, variance, etc) of the resulting PDF of the damage location parameters.

Based on the efforts described in this work, a number of conclusions can be drawn:

First, a SHM method that accounts for uncertainty in the SHM problem in a structured fashion has been successfully established. Second, the Monte Carlo simulation is suited to model uncertainties when dealing with statistical analysis. Third, the probabilistic approach is capable of showing the effect of the level of uncertainties on the damage localization, which proves that the damage localization is more sensitive to the stochastic uncertainty than the model uncertainty, implying that the elastic wave energy decay model is accurate and robust. Also, a conclusion can be drawn that the key aspect of the probabilistic approach is the minimization of false-positive and false-negative indicators from the damage localization process. False- positive refers to the situation where damage is indicated when in fact none is present. False- negative refers to the situation where damage is not indicated, even though it is present. Fourth, the method is an active damage detection technique, which is suitable for the applications of SHM. Lastly, the method uses the all time series data information

collected by each sensor, not only the time-of-flight or time of arrival. Experimental and simulation results show that the estimated damage location by least-squares method makes good agreement with the targeted location.

A Probabilistic Approach to Damage Localization in Structural Health Monitoring

by

Hussein Said Harb

A thesis submitted to the Graduate Faculty of
North Carolina State University
in partial fulfillment of the
requirements for the Degree of
Master of Science

AEROSPACE ENGINEERING

Raleigh, North Carolina

2005

Approved by:

Dr. F. G. Yuan

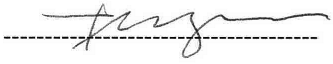

Dr. K. Peters

Dr. J. Eischen

To my parents

and

those who inspired me

Biography

Hussein Said Harb was born on May 6, 1981 in Burj El Brajneh, Lebanon. He is the son of Said Harb and Amera Harb and the brother of Nahed Harb, Kasem Harb and Mohammad Harb, all of Burj El Brajneh, Lebanon. He finished his high school education from Amlieh High school in Beirut, Lebanon. He moved from Lebanon to North Carolina in January 6, 2000 to begin his college career at North Carolina State University. He completed his Bachelor of Science Degree in Aerospace Engineering at North Carolina State University in May of 2003. In the fall of 2003, he joined the masters program of Aerospace Engineering at North Carolina State University at Raleigh. Upon the completion of his thesis requirements in May 2005, Hussein Harb will begin employment at Gulfstream Aerospace Corporation in Savannah, Georgia.

Acknowledgments

I would like to thank Dr. F. G. Yuan for suggesting the following work and serving as my graduate advisor over the last two years. I appreciate the support and encouragement that Dr. Yuan has given me through out all the years that I have known him. Also, I would like to thank my committee members, Dr. Jeffery Eischen and Dr. Kara Peters, for serving on my committee and readying this thesis. This research is supported by the National Science Foundation.

As for my fellow graduate students, thanks go to Mr. Saeed Nojavan (and his wife), who I shared almost all my time with him in the office. I would like to give him my sincere appreciation for all the time that he spent to answer my questions. Also, I would like to thank him for all the advice and the support that he provided me throughout the last three semesters. Thanks go to Mr. Lei Wang who was very nice to answer most of my questions and to provide me with the experimental and simulation data that I needed for this work. Thanks go to Mr. Nate Pringle who gave me the support that I needed to make my life easier in Raleigh and at North Carolina State University. Thanks go for the rest of Dr. Yuan's group: Mr. Lei Liu, Mr. Jin Yun, and Mr. Guoliang Jiang.

I would like to thank Ms. Christy Layton and her family. Ms. Christy Layton is a very special person to me. I owe her my life. She is the reason for my success. Her love, kindness, lovely personality, moral and financial support were the reason for my success here in North Carolina. To Christy:

"Khedne Ma'ak Ala Darb Be'ed, Matrah Ma kena Wlad Zghar

Dafe Rabe'e Bshams Jded, Wnasene elyawm elserna Kbar"

Thanks go to Mrs. Ana Maria Star and Mr. Jason Star. I am so blessed to have such a wonderful friendship with you guys. Thanks go to Mr. Steve Bischoff, Mr. Kayode Ariwedolla, Mr. Maher Harb, Mr. Medhat Karout, and Mrs. Ranim Karout for their encouragement and support to continue my education and for all the time that we spent together during my stay in North Carolina.

Finally, words are not enough to thank my father, my mother, my two brothers, and my sister Nahed Harb including her husband Ali Safa and her two angels Hassan and Adam. My parents: you are the light that brightens my life. If it was not for your love and support, I would not be able to achieve my goals. To my family:

"Sail your smile to the air; it will reach and enliven me!

Breathe your fragrance into the air; it will sustain me!"

Khalil Gibran

Table of Contents

List of Tables

List of Figures

Nomenclature and Abbreviations

Greek Symbols

α	Reflection factor at the damage
γ	Sensor gain factor at a sensor
μ	Mean
$\boldsymbol{\rho}$	Damage position vector
$\mathbf{P}$	Probability density function for the damage position vector
$\mathbf{P}_x$	Probability density function for the damage position along the *x*-axis
$\mathbf{P}_x$	Probability density function for the damage position along the *y*-axis
σ	Standard Deviation
ς	Updated step size in least-squares algorithm
τ	Time delay from the actuator to the damage
ω	Angular frequency
ψ	Mother wavelet or base wavelet function
ζ	Outcomes

Roman Symbols

a_0	Normalized reflected wave form from damage
$\boldsymbol{a}_0$	Probability density function for the normalized reflected wave
c_g	Group velocity
c_p	Phase velocity

E	Young's modulus
F_X	Cumulative Distribution Function
f	Frequency
$\mathbf{X}$	Probability Density Function
f_s	Sampling rate
g	Square of sensor gain factor at a sensor
h	Thickness of the plate
J	Least-squares error function
$\boldsymbol{J}$	Probability density function for the least-squares error function
P	Probability
q	Five-peak excitation signal
$\boldsymbol{r}$	Cartesian coordinates of a sensor
s	Modeled received signal without additive noise at a sensor
t	Time variable
x, y, z	Cartesian coordinates
x	Modeled received signal with additive noise at a sensor
x	Real Number
X	Random Variable
$\hat{y}$	Modeled wave energy at a sensor
$\hat{\mathbf{Y}}$	Probability density function for the modeled wave energy at a sensor
y	Measured wave energy at a sensor
$\mathbf{Y}$	Probability density function for the measured wave energy at a sensor

Subscripts

c	Denotes central frequency
m	Sensor number
x, y	Components along the direction of Cartesian coordinates

Superscripts

i	Epoch of the least-squares algorithm
+	Right

Caps

–	Mean

Abbreviations

2D	Two Dimensional
CDF	Cumulative Distribution Function
CEV	Crew Exploration Vehicle
DOA	Direction of Arrival
MLCG	Multiplicative Linear Congruential Generators
NDE	Non-destructive Evaluation
PDF	Probability Density Function
PZT	Lead Zirconate Titanate
RNG	Random Number Generator
SDE	Stochastic Differential Equation
SHM	Structural Health Monitoring
Std	Standard Deviation

1 Introduction

1.1 Why Structural Health Monitoring?

On April 28, 1988, an Aloha Airlines Boeing 737 suddenly lost an upper fuselage section while at 24,000 feet. Sixty-nine passengers were injured and one flight attendant was swept from the plane. Inspections of the aircraft in the aftermath of the accident revealed significant multiple site damage in the fuselage fastener hole. The suspected cause of the damage was corrosion fatigue. Ironically, within the six month prior to the accident, the plane had been inspected and undergone some minor repair work in accordance with the FAA and Boeing guidelines (Vanik, 1997).

On June 17, 2002, the wings came off a Lockheed C-130A firefighting tanker as it pulled up from dropping extinguishing agent on a blaze near Walker, California, killing all three crews (Aviation Week & Space Technology, 2002). Videotape of the accident showed that both left and right wing panels folded up at the wing root and departed the aircraft, with the fuselage hitting the ground roughly 5 sec. later. Inspections of the fighter aircraft revealed a 10-12 in. fatigue crack in the center wing box of the firefighting Lockheed C-130A along the line where the right wing was separated from the body. Other smaller fatigue cracks were also found along the parting line on the lower wing skin.

These are a few of other available examples wherein structural failure arose due to loss of structural integrity. These examples also revealed that existing inspection regulations and techniques were insufficient to locate the hidden cracks and to recognize the possible danger in a timely and detailed manner. Therefore, a technique, which is able to monitor the state of a structure in a detailed manner, more acceptable time scale, warn of potential

problems, and locate the invisible damages, would improve structural safety. This leads to a great deal of research in the area of Structural Health Monitoring.

1.2 Structural Health Monitoring

Structural Health Monitoring, or SHM for short, is the process of establishing some knowledge of the current physical condition of a structure. The essence of SHM technology is to develop autonomous built-in systems for the continuous real-time monitoring, inspection, and damage detection of structures with minimum labor involvement (Chang, 1997). A successful technology for SHM has enormous potential for applications in monitoring aerospace structures subject to fatigue, corrosion, or impacts, earthquakes, as well as building, offshore structures, and bridges subject to severe loads or structural deterioration.

A great deal of research in SHM has begun in the past thirty years, aiming at establishing effective methods for health monitoring in civil, mechanical, and aerospace structures. In particular, for real applications of SHM in aerospace, Boeing's new 787 aircraft will have a full-time built-in SHM system with sensors embedded in the structure to evaluate the state of structural health. According to NASA's requirements on the new Crew Exploration Vehicle (CEV), Lockheed Martin's Atlas V and Boeing's Delta IV satellite launchers will soon have integrated health-monitoring system to assess the overall health of the vehicle continually during the ascent to spot a problem before it becomes catastrophic (Lannotta, 2004).

The potential benefits from a SHM system are enormous such as real-time monitoring and reporting, saving in maintenance cost, reducing labor, downtime and human error, improving safety, reliability, and etc.

In order to convey an appreciation for the nature of the research in SHM, this section presents a brief description of a few techniques developed to detect various forms of damages in both local and global approaches.

Local Damage Identification

Local SHM techniques use direct examination of structural members to determine the condition of those members. Many methods fall into this class. Visual inspection is the most basic form of local SHM. In certain cases, visual inspections are complemented by non-destructive testing procedures but these are local in nature and cannot provide information on the overall health of the structural system. A good example of the limitations of SHM technology based on visual inspection is found in the damage induced by the 1994 Northridge Earthquake on welded moment-resisting connections of steel buildings (Vanik, 1997). Needless to say, given the cost and difficulty of inspecting hidden structural elements and connections, detailed inspection was not carried out first. Detailed inspection of existing structures showed that the type of weld fractures that had been observed was pervasive in the existing building stock. The situation, if undetected, would have resulted in a significant number of weakened buildings that would pose undue risk to the occupants during future earthquakes.

In order to assist with detecting small-scale faults, non-destructive evaluation (NDE) techniques can be employed. Eddy current and magnetic flux approaches look for cracks and delaminations (for composite materials) by monitoring impedance changes in a coil placed

near the surface of the structure (Vanik, 1997). Ultrasonic techniques send high frequency waves into a member and measure the backscatter signals. The backscatter signals carry information about discontinuities such as cracks, delaminations, and other defects. While these NDE methods provide a good picture of the member under consideration, there are a few limitations. First, the NDE techniques have the same problem as visual inspection as regards to inaccessible areas. Also, applying these procedures are quite difficult, expensive and time-consuming. Finally, these approaches require an inspector to be present to conduct the investigation (Vanik, 1997).

Another set of local SHM techniques, which do not require user interaction, have also been developed. Such methods address the problems of monitoring difficult-to-access components of a structure and of increasing the rate of monitoring by placing sensors either directly on structural members or embedding them in the structures and monitoring them remotely. Besides sensors, actuators exciting diagnostic signals can also be surface-mounted on or embedded in the structures to build an active SHM system. A major advantage of the active SHM system over a passive one (without built-in actuators) is that the active SHM is subjected to a prescribed actuation and thus increases the accuracy and reliability of assessing the structural status from the collected sensor data (Wang, 2004).

Generally, the excitation in an active structural health monitoring system (with both sensors and actuators) can be mechanical and non-mechanical. Mechanical signals, such as elastic and acoustic waves, are those for which a mechanical medium is needed for propagation, i.e. solid, fluid or gas medium. On the other hand, a non-mechanical wave, such as electromagnetic wave, can propagate in any medium including vacuum. Wave-based damage detection technique excites transient waves propagating into structures by actuators,

since the waves will be reactive to damages such as reflection, scattering or dissipation, the health status of structures will be estimated by analyzing the response waves received by the sensors. Wave-based method can effectively obtain the local information of structures and can accommodate variations of boundary conditions and temperatures (Sohn *et al*., 2004).

All of these local techniques can give indication of the location and possible severity of the damage in the area to which they are applied. By application to the high stress areas, these local methods could provide a very complete picture of the current damage state of the structure. For small regular structures such as pressure vessels and wing boxes, this might be a reasonable application of these local approaches. For structures beyond a certain size and complexity, examination of every component of the structure is not feasible. These methods are therefore best used to monitor specific components of a structure.

Global Damage Identification

Numerous investigators have applied vibration-based methods to detect damage existence and attempt to localize damages mainly in rotating machinery or civil structures such as bridges, highways, and buildings. However, there are several essential disadvantages limiting the extensive application of vibration-based damage detection methods:

First, vibration-based approaches have low sensitivity to damage. The basic premise of most vibration-based damage detection methods is that damage will alter the physical parameters such as stiffness, flexibility, damping, etc., which in turn alter the measured dynamic response of the structure such as resonant frequencies and mode shapes. However, the damage is typically a local phenomenon, at least in the beginning stage, and may not

significantly influence the global response of a structure that is normally measured from the vibration test.

Second, a limited number of lower modes and truncated mode shapes that can be reliably determined can lead to systematic error. In vibration-based methods, the response measurement can be expressed in terms of a superposition of all mode shapes, but only a limited number of modes may be accessible in practice because of limited number of sensor measurements and loss of fidelity in higher modes.

1.3 The Basic Concept of Probability

Engineers face uncertainty consciously and/or unconsciously when they perform the engineering design. Generally speaking, engineering uncertainties (that will be discussed in detail in Section 2.4) may occur in three basic ways.

Uncertainty occurs when engineers measure parameters or make predictions of dependant variables from measured quantities. Engineers are inclined to assume that this kind of uncertainty does not exist at all. They tend to treat problems of this type as determinate, and over-design to compensate for uncertainty. This must be considered as a rather crude treatment of this kind of uncertainty, and we must learn how to bring our judgment to bear on the problem in a more rational way, using the concepts of probability theory (Siddall, 1983).

The second basic type of engineering uncertainty occurs when we are concerned with an event that may or may not occur, or the time of its occurrence may be uncertain (Siddall, 1983).

Engineers may also be uncertain about the validity of a hypothesis or theory that is to be used to predict performance of an engineering design.

To deal with uncertainty in a rational and ordered manner, we must be able, in a sense, to measure it. The term *event* will be used to designate all the kinds of phenomena that are uncertain. The measure of the degree of uncertainty about the likelihood of an event occurring is probability. In an attempt to measure probability, we begin by arbitrarily defining its range as 0 to 1 (0 to 100%). If we are certain that an event will not occur, we say that it has a probability of 0; if we are certain that an event will definitely occur, it has a probability of 1.

1.4 Why Probability in Structural Health Monitoring?

In locating the damage, if the data collected by the sensors have very low noise levels and the damage localization algorithms are rigorous, no significant uncertainty may be present. Ignoring the uncertainty should not lead to any problems. However, in many cases, these assumptions do not apply. The algorithms rarely capture the full behavior of the structure. Further, the amount of sensor data is limited. In addition, even when the sensor data are available, it tends to show significant variation from one measurement to the next (Vanik, 1997). In this case, the uncertainty issue cannot be avoided. Uncertainties will lead to difficulties in concluding whether changes in the model parameters are due to damage or effect of uncertainty. Due to different types of uncertainties that are due to noise in the measurements, environmental changes, human error, modeling error, and etc. (more details in Section 2.4), a method should be used to quantify and assess the different types of uncertainties. Thus a method that is capable of measuring the degree of belief of the damage location by taking uncertainties into account should be used to make decisions concerning

structural safety and quantifying the sensitivities of various uncertainties. Probability analysis is a method that can achieve this objective.

1.5 Previous work in SHM considering Uncertainties

Vanik, Beck, and Au (2000) presented a Bayesian probabilistic methodology for global damage detection in bridges. The method used a sequence of identified modal parameter data sets to continuously update stiffness parameters. The probability of the updated stiffness parameters being less than a specified fraction of the corresponding initial model stiffness parameters is calculated. In this approach, a high likelihood of reduction in model stiffness at a location is taken as an indicator for damage at the corresponding structural location. A damage metric is used as the changes in the stiffness parameters that are identified from modal parameter data sets, between an undamaged state and a possibly damaged state. This measure is needed because several factors such as variation in the identified modal parameters even in the absence of damage as well as unavoidable model error can lead to uncertainties in the updated modal parameters.

Baruh and Ratan (1993) developed a method for the identification of structural damage and detection of the location of damage in a truss structure. The detection was carried out in two parts. First, the eigensolution of the system was identified using a modal parameter identification technique. Then, the identified eigensolution was used together with the properties of the eigenvalue problem to detect the damage components. A sensitivity analysis was performed, where the effects of uncertainty in the mathematical model were analyzed. For example, they considered an original model, which is incorrect in the mass and stiffness properties for all the truss elements: they increased the level of uncertainty and

compared the accuracy of the damage localization. The results indicated that if there are modeling uncertainty in all the truss elements over 10%, the damage localization results are not very accurate. It was observed that such uncertainty, when moderately small, do not affect the damage localization results.

Sohn *et al.* (2001) presented structural health monitoring in the context of a statistical pattern recognition paradigm. Two pattern recognition techniques based on time series analysis were applied to fiber optic strain gauge data obtained from two different structural conditions of a surface-effect fast patrol boat. The first technique was based on a two-stage time series analysis combining Auto-Regressive (AR) and Auto-Regressive with exogenous inputs (ARX) prediction models. The second technique employed an outlier analysis with the Mahalanobis distance measure. The Mahalanobis squared distance of the outlier was checked against a threshold value. A Monte Carlo method was used to define the threshold value. Due to the uncertainties, they used data normalization as a procedure to "normalize" data sets such that signal changes caused by operational and environmental variations of the system can be separated from structural changes. The main objective of the work was to extract features and construct a statistical model that distinguishes the signals recorded under the different structural conditions of the boat. These two techniques were successfully applied to the patrol boat data clearly distinguishing data sets obtained from different structural conditions.

Fugate *et al.* (2000 and 2001) also presented vibration based-damage detection problems in the context of statistical pattern recognition. Statistical process control using control charts was applied in an unsupervised learning mode to the vibration test data obtained from the bridge column in its undamaged state and after various levels of damage

has been introduced. In their work, they focused on applying statistical process control methods referred to as "control charts" to vibration-based damage detection. First, an auto regressive (AR) model was fit to the measured acceleration-time histories from an undamaged structure. Residual errors, which quantify the difference between the prediction from the AR model and the actual measured time history at each time interval, were used as the damage-sensitive features. Next, the X-bar and S-control charts were employed to monitor the mean and variance of the selected features. Control limits for the control charts were constructed based on the features obtained from the initial intact structure. The residual errors computed from the previous AR model and subsequent new data were then monitored relative to the control limits. A statistically significant number of error terms outside the control limits indicated a system transit from a healthy state to a damage state. In their work, two key issues raised when attempting to apply the statistical procedures to SHM. First, one must examine features that quantify environmental and operational variability as well as the structural condition. Without this measure, one will have difficulty distinguishing changes in vibration response caused by damage from changes caused by other sources of variability. Second, the addition of these environmental and operational features must be done with the concept of feature vector dimensionality in mind. Therefore, the environmental uncertainties were incorporated directly into the AR model by adding a parameter for each factor of interest along with observed values of the factor.

Doebling *et al.* (1998) studied the issue of the statistical significance of the changes in the modal parameters and damage indicators between the various damage cases in the I-40 bridge experiments. The emphasis was to determine the statistical significance of the changes from one case to case. The approach demonstrated in their work uses Monte Carlo analysis to

compute statistical confidence intervals on the mode shape components and damage indication parameters. Then a statistical difference test was employed to associate a confidence level with the statement that the mean values between the two sample sets were significantly different. This statistical difference tests was applied to the individual flexibility change at that particular degree of freedom should be considered to be statistically significant or not. These difference statistics indicated the relative significance of the changes in a particular parameter relative to changes in other parameters. The shortcoming of their work is that uncertainties were not considered. Therefore, the results of their analysis can only discriminate whether the observed changes are statistically significant, not whether the source of the observed changes is structural damage. For example, a systematic error in the testing procedure or a change in the structural boundary conditions can both lead to a statistically significant change in the measured structural flexibility, which the analyst may falsely conclude is the result of structural damage.

1.6 What Does This Work Present?

This work presents a probabilistic methodology for damage localization in plate-like structures. This probabilistic methodology incorporates different types of uncertainty (which is discussed in detail in Section 2.4) in the SHM process. The mathematical description and quantification of uncertainty is described in Section 2.5. Also, the effect of the level of uncertainties on damage localization is analyzed.

Determining the physical condition of the structure that is based on finite numbers of sensor measurements is a nonlinear inverse problem. Solutions to the inverse problems are inherently unstable or ill-posed, i.e., the solution is sensitive to noise and measurement error.

In addition, inverse problems are non-unique due to the fact that complete data collection is not practically feasible. To solve this nonlinear problem, which is sensitive to signal-to-noise ratio and measurement error that leads to uncertainties, a damage localization technique based on a least-squares method and Monte Carlo simulation considering uncertainties is mathematically developed. The estimated damage location may be calculated from collected signals such that the error function between the estimated damage location and the real location reaches its minimum. The least-squares damage localization technique utilizes the signals reflected from a single damage and iteratively searches damage position until the error function reaches its minimum value.

In a previous work done by Mr. Wang at North Carolina State University, an active structural health monitoring system (with both sensors and actuators) is used. The actuators are used to excite elastic waves. Also, the least-squares method has been mathematically deduced and verified *via* both numerical simulation and experiments. This technique was demonstrated through the following steps:

- An elastic wave energy decay model for wave propagating in plates was established.
- The least-squares method was applied to iteratively search localized damage based on minimization of the difference between the measured and the modeled elastic wave energies.
- Simulation examples for single damage detection were demonstrated using Matlab.

- A simple experimental system was set up to validate the feasibility of the least-squares method for damage localization in an aluminum plate.

From the simulated results and experimental data, it was shown that the estimated damage position by the least-squares method gave good agreement with the targeted damage location.

In this work, the least-squares method for damage localization is used in a probabilistic framework. Uncertainties using Monte Carlo simulation will be incorporated in the analysis and in all the steps mentioned above. This method is verified *via* numerical simulation and experimental data. The goals of this method are accomplished by formulating the solution in a probabilistic framework, which takes two types of uncertainties into account. Also, in the following, uncertainty of a quantity is described in terms of a Probability Density Function (PDF) that specifies the probability of all possible values of that quantity. In this context, probability is used as the quantitative measure of the degree of confidence of the damage location by taking uncertainties into account. For engineering applications, representing the uncertainty as probability information is reasonable because large amounts of test data and well-established formal theories are available.

The basic procedure of the probabilistic approach and the Monte Carlo method used in this work can be summarized as the following: *"The objective of the problem is to deduce the probabilistic means of the damage location from the probability density functions of the measurements and the model"*. Due to the complexity of the mathematical relation in the equations between the inputs and the output, the Monte Carlo method is used.

Some simple problems have been examined to solve for the resultant PDF of a certain outcome using the PDF of certain inputs. One example is illustrated in detail as follows.

Nowak *et al.* (2000) presented a cantilever beam such shown in the following figure.

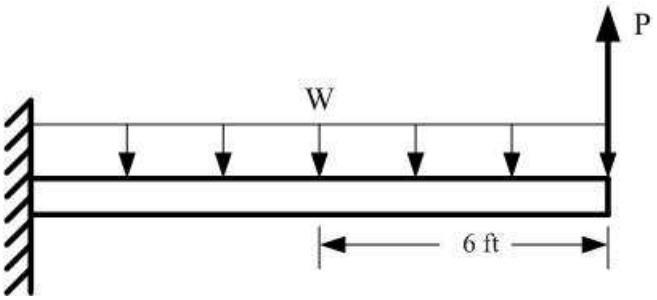

Figure 1.1 Example of a cantilever beam

Using the Monte Carlo technique, the mean and the standard deviation of the moment of 6 ft from the free end is to be calculated. The loads P and W are independent normal random variables with the following parameters:

$$\overline{P} = 4000\,\text{lb}\ ,\ \overline{W} = 50\,\text{lb/ft}$$

$$\sigma_P = 400\,\text{lb}\,,\ \sigma_W = 5\,\text{lb}/\text{ft}$$

The bending moment M at the location of interest is $M = 6P - 18W$. Since P and W are both independent normal random variables and M is a linear function of P and W, thus M is also a random variable. The mean and the standard deviation of M can be calculated exactly by using the following formulas:

If $Y = a_0 + a_1X_1 + a_2X_2 + \cdots + a_nX_n = a_0 + \sum_{i=1}^{n} a_iX_i$ where $a_i\ (i = 0,1,\ldots,n)$ are constants and X_i are random variables. Then the mean of Y is $\overline{Y} = a_0 + \sum_{i=1}^{n} a_i\overline{X}_i$ and the variance of Y is $\sigma_Y^2 = \sum_{i=1}^{n} a_i^2\sigma_{X_i}^2$

Therefore:

$$\overline{M} = 6\overline{P} - 18\overline{W} = 23100\,\text{lb}\cdot\text{ft}$$

$$\sigma_M = \sqrt{(6\sigma_P)^2 + (18\sigma_W)^2} = 2400\,\text{lb}\cdot\text{ft}$$

The exact solution was compared with the Monte Carlo solution. For this example, five values of the bending moment M will be calculated using the Monte Carlo simulation. Therefore, five values of the load P and five values of the load W will be simulated. This will require determining 10 values (two simulated variables times five values of each variable) of a uniformly distributed random variable u_i between 0 and 1. The uniform random numbers are generated and then the simulated values of P and W are calculated using the equation $x_i = \overline{X} + z_i\sigma_X$. Therefore, for a given sample value z_i, the corresponding x_i value can be calculated. The following table corresponds to the values of P and W that have been calculated.

u_i	z_i	$P_i = 4000 + z_i(400)$
0.050203	-1.64289	3343
0.619129	0.303194	4121
0.872402	1.13782	4455
0.376568	-0.31451	3874
0.139927	-1.08065	3568

u_i	z_i	$W_i = 50 + z_i(5)$
0.318491	-0.47192	47.64
0.987671	2.24672	61.23
0.033265	-1.83483	40.83
0.234626	0.723697	46.38
0.623157	0.313783	51.57

Next, five data sets $\{P_i, W_i\}$ are formed and used to generate five values for the moment M using $M_i = 6P_i - 18W_i$. The following results are generated for M_i (lb.ft), (19200, 23620, 25990, 22410, 20480). Then the mean and the standard deviation can be calculated using the following equations:

$$\overline{M} = \frac{1}{5}\sum_{i=1}^{5} M_i = 22{,}340\,\text{lb}\cdot\text{ft}$$

$$\sigma_M = \sqrt{\frac{(\sum_{i=1}^{5} M_i^2) - 5(\overline{M})^2}{5-1}} = 2659\,\text{lb}\cdot\text{ft}$$

Comparing these values with the theoretical exact values obtained earlier, it can be noticed that the values are comparable but not as accurate as they should be. The accuracy of the Monte Carlo simulation approach increases as the number of sample values increase. If more simulated values of M are generated, the estimate of the mean and the standard deviation would improve. For example, when the number of samples is 50, the sample mean and standard deviation are found to be 22990 lb.ft and 2332 lb.ft respectively. These values are much closer to the theoretically correct values of 23100 lb.ft and 2400 lb.ft.

2 Theoretical Background and Mathematical Formulation

2.1 Probability and Random Variables

Probability is a scale of measurement used to describe the likelihood of an event, where an event is defined as the occurrence of a specified value of a random variable, e.g., the location of damage.

$$P(X = x_0) = \frac{n}{N}$$

where n is the number of observations on the random variable X that results in an outcome of interest x_0, and N is the total number of observations of X.

In any experiment there are numerous phenomena that can be observed or measured. In general, each outcome of an experiment can be associated with a number by specifying a rule of association. Such a rule of association is called a random variable. Therefore, a random variable assigns numerical values to the outcomes of an experiment.

2.2 Histogram, Cumulative Distribution Function, Probability Density Function.

Histogram is a special type of charts that are commonly used to display and describe data. They are developed from that data for some variables of interest. A histogram is a plot of the number of data points of occurrence versus selected intervals or values for a parameter.

Given a real number x, the set $\{X \le x\}$, consisting of all outcomes ζ such that $X(\zeta) \le x$, is an event. Its probability $P\{X \le x\}$ is a number depending on x; that is, a function of x. This function is denoted by $F_X(x)$ and is called the cumulative distribution function (CDF) of the random variable X. Therefore, the CDF of a random variable X is the

function $F_X(x) = P\{X \le x\}$ defined for any number x from $-\infty$ to $+\infty$. Thus, for a given x, $F_X(x)$ represents the probability of the event $\{X \le x\}$consisting of all outcomes ζ such that $X(\zeta) \le x$. The CDF $F_X(x)$ has the following properties:

- $F_X(-\infty) = 0, \quad F_X(+\infty) = 1$
- It is a non-decreasing function of x: $F_X(x_1) \le F_X(x_2)$ for $x_1 < x_2$
- It is continuous from the right: $F_X(x^+) = F_X(x)$

The derivative $\mathbf{X} = \dfrac{dF_X(x)}{dx}$ of the CDF $F_X(x)$ is called the probability density function (PDF) of the random variable X. $\mathbf{X}$ is a non negative function and $\int_{-\infty}^{+\infty} \mathbf{X}\, dx = 1.$

A typical example of the PDF is the Gaussian distribution. Experimental measurements always contain some variability, thus no conclusion can be drawn with certainty. Statistics gives us tools to accept conclusions that have a high probability of being correct and to reject conclusions that do not. If an experiment is repeated many times, and if the errors are purely random, then the results tend to cluster symmetrically about the average value. The more times the experiment is repeated, the more closely the results approach an ideal smooth curve called the Gaussian distribution. The Gaussian distribution function is given by the simple formula:

$$\mathbf{X} = \frac{1}{\sigma\sqrt{2\pi}} \exp\left(-\frac{(x-\mu)^2}{2\sigma^2} \right) \qquad (2.2.1)$$

where x represents the possible outcome of the measurement. The quantity μ is the mean value of the measurements and σ is the standard deviation (variance) of the measurement set. The function **X** determines the probability of the occurrence of the outcome x of the measurement. The mean and standard deviation characterize the Gaussian distribution. The mean is the center point of the curve and the standard deviation measures how closely values are clustered about the mean. Figure 2.1 shows the Gaussian distribution with a mean μ and a standard deviation σ.

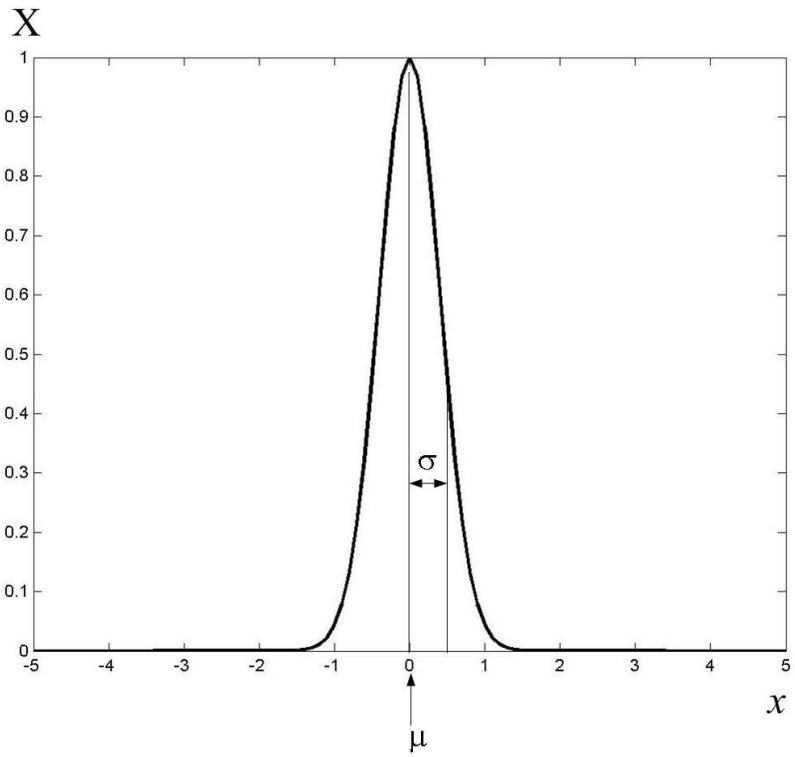

Figure 2.1 Gaussian distribution with mean $\mu = 0$ and standard deviation $\sigma = 1/\sqrt{2\pi}$

2.3 Joint Distribution Function of Two Random Variables

If X and Y are two random variables, the joint distribution function of X and Y, denoted by $F_{XY}(x, y)$, is defined as the probability of the intersection of two random events $\{X \le x\}$ and $\{Y \le y\}$:

$$F_{XY}(x, y) = P\{(X \le x) \cap (Y \le y)\} = P(X \le x, Y \le y) \tag{2.3.1}$$

treated as a function of two random variables x and y. $F_{XY}(x, y)$ is sometimes called the joint cumulative distribution function of X and Y. If $F_{XY}(x, y)$ is the joint (cumulative) distribution function of X and Y, then the distribution functions $F_X(x)$ and $F_Y(y)$ are called marginal distribution functions.

Consider $F_{XY}(x, \infty) = P(X \le x, Y \le \infty) = P(X \le x) = F_X(x)$ (2.3.2)

Since $Y \le \infty$ is a certain event and $(X \le x, Y \le \infty) = (X \le x)$. Similarly,

$$F_{XY}(\infty, y) = P(X \le \infty, Y \le y) = P(Y \le y) = F_Y(y) \tag{2.3.3}$$

Geometrically, the joint probability distribution function $F_{XY}(x_1, y_1)$ represents the probability of a random point (a point with random coordinates X and Y) falling within the quadrant bounded by lines $x = x_1$ and $y = y_1$ intersecting at (x_1, y_1) as shown in Figure 2.2a. The marginal probability density $F_X(x_1)$ is the probability of the abscissa of the random point falling to the left of $x = x_1$ (Figure 2.2b), and $F_Y(y_1)$ that of it falling below $y = y_1$ (Figure 2.2c). Falling anywhere in the xy plane is a certain event; hence,

$$F_{XY}(\infty, \infty) = 1 \tag{2.3.4}$$

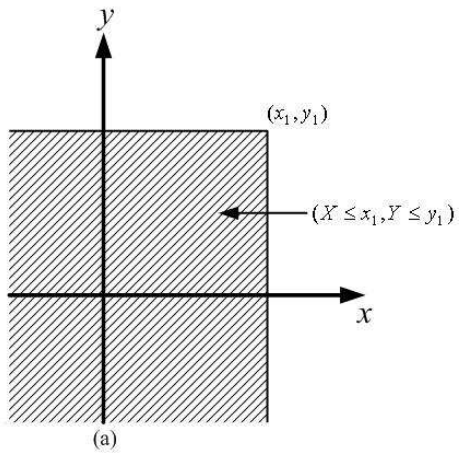

Figure 2.2 (a) Joint probability distribution function $F_{XY}(x, y_1)$ is described by the probability of the random point falling within the shaded area. (b,c) The marginal distribution function $F_X(x_1)$ and $F_Y(y_1)$, respectively, are described by the probability of the random point falling within the shaded areas

The joint probability distribution function approaches zero as either or both of its arguments, *x*, *y* approaches $-\infty$:

$$F_{XY}(-\infty, y) = F_{XY}(x,-\infty) = F_{XY}(-\infty,-\infty) = 0 \tag{2.3.5}$$

Indeed, since $\{X \le -\infty, Y \le y\} \subset \{X \le -\infty\}$ we have $\mathrm{P}\{X \le -\infty, Y \le y\} \le \mathrm{P}\{X \le -\infty\} = 0$ which leads to the first of the equalities in equalities 2.3.5, other equalities are derived in an analogous manner. Geometrically, Eq. 2.3.5 is quite clear: As one of the arguments *x* or *y*, approaches $-\infty$, the probability of the random point falling within the shaded quadrant approaches zero.

Now suppose $x_1 < x_2$. We have, then, for a fixed $y = y_2$,

$$P(x_1 < X \le x_2, Y \le y_2) = P(X \le x_2, Y \le y_2) - P(X \le x_1, Y \le y_2)$$

which is illustrated in Figure 2.3.

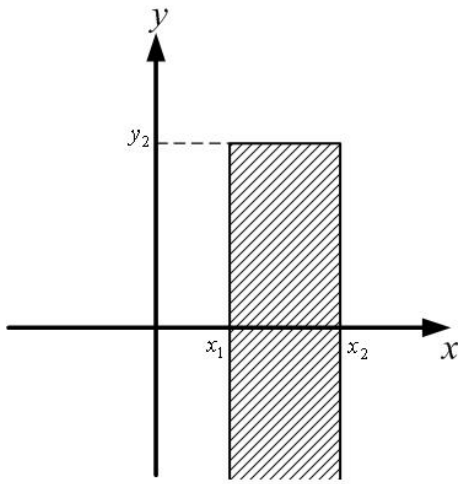

Figure 2.3 Probability of random point falling within the shaded area is described by the difference

$$F_{XY}(x_2, y_2) - F_{XY}(x_1, y_2)$$

We have

$$P(x_1 < X \le x_2, Y \le y_2) = F_{XY}(x_2, y_2) - F_{XY}(x_1, y_2) \tag{2.3.6}$$

Since the left-hand term of Eq. 2.3.6 is a probability, it is a nonnegative, implying that the joint probability distribution function is a non-decreasing function of *x*. Similarly, it is a non-decreasing function of *y*; indeed, if $y_1 < y_2$ we have, for fixed $x = x_2$ (see Figure 2.4)

$$P(X \le x_2, y_1 < Y < y_2) = P(X \le x_2, Y \le y_2) - P(X \le x_2, Y \le y_1)$$

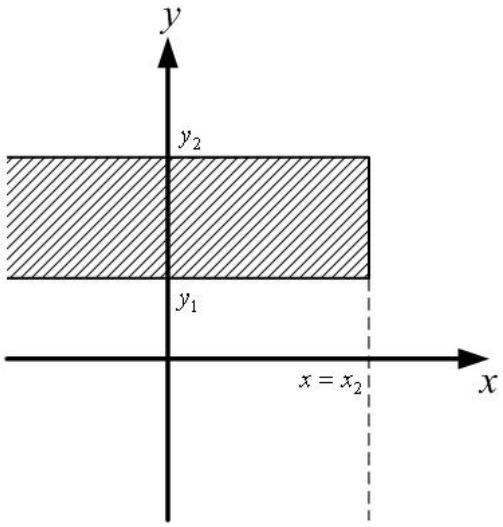

Figure 2.4 Probability of random point falling within the shaded area is described by the difference

$$F_{XY}(x_2, y_2) - F_{XY}(x_2, y_1)$$

The rectangle in Figure 2.5 may be considered as the difference of two half-strips, so that

$$\begin{aligned} P(x_1 < X \le x_2, y_1 < Y \le y_2) &= [F_{XY}(x_2, y_2) - F_{XY}(x_2, y_1)] - [F_{XY}(x_1, y_2) - F_{XY}(x_1, y_1)] \\ &= F_{XY}(x_2, y_2) - F_{XY}(x_1, y_2) - F_{XY}(x_2, y_1) + F_{XY}(x_1, y_1) \end{aligned} \quad (2.3.7)$$

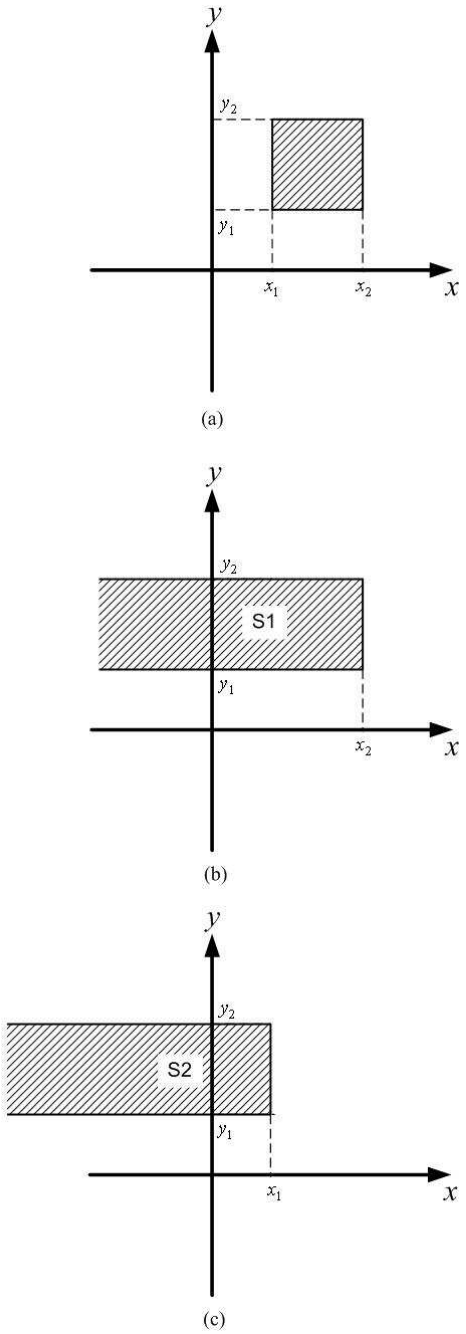

Figure 2.5 (a) Probability of a point falling within the rectangle is described by the difference of those of it falling within half-strip S1 (b) and half-strip S2 (c), as per Eq. (2.3.7)

2.4 Definitions and Classification of Uncertainty

Uncertainty can be defined as the potential deficiency that is due to the lack of knowledge. In general, the uncertainty can be categorized into four different types as shown in Figure 2.6:

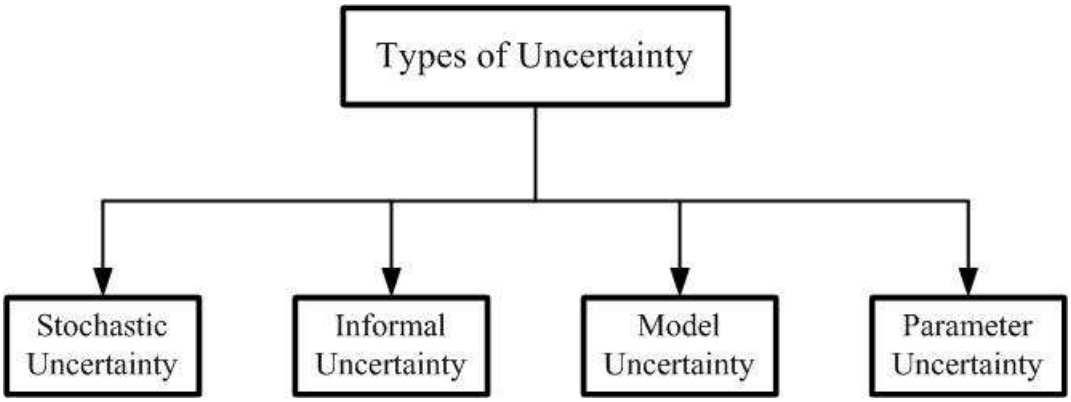

Figure 2.6 Types of Uncertainty

Stochastic uncertainty (Moller, 2004) exists due to presence and change of environments, operating interference, and acoustic/electrical noise. In experiment, this uncertainty can be described as a future data that cannot be predicted within reasonable experimental error. An engineer or an analyst working with experimental data needs to run an experiment several times to validate the experimental output. In most cases, an engineer would notice a variation in the output at every experiment. This is due to the stochastic uncertainty, considering that all the setup of the experiment is held the same.

Informal uncertainty (Moller, 2004) results from an information deficit. In other words, informal uncertainty or subjective uncertainty (Ayyub, 1994) is based on the limited insufficient information about the system and expert-based assessment of engineering structures.

Model uncertainty is an uncertainty in the physical model. This kind of uncertainty usually occurs when the physical model is used to predict the actual behavior of the real structure. For example, simulating a plate girder (Kim and Stubbs, 1995), using finite element methods, would produce model uncertainty due to the fact that choosing a specific type of element in finite elements may not truly represent the real behavior of the structure. Assuming an isotropic and perfectly clamped model to represent an isotropic clamped cantilever beam can also generate model uncertainty because in the real case, the beam would not be perfectly clamped or isotropic. Simplifying assumptions about geometry of the structure and physical behavior, in the process of developing the physical model are another examples of model uncertainty.

Parameter uncertainty is uncertainty about the actual value of a parameter in the mathematical model of the real system. Parameter uncertainty has no influence on the physical model. After selecting the physical model, the parameters included in the mathematical model, should be analyzed to detect the uncertainties in these parameters. For example, stiffness parameters of a real structure can be unknown (Kim and Stubbs, 1995), so when considering the stiffness parameters in the mathematical model, these parameters can fall under the parameter uncertainty category.

2.5 Uncertainty Analysis

Methods including probabilistic methods, non-probabilistic methods, moment methods, stochastic differential equation methods, etc., are available for the mathematical description and quantification of uncertainty

Uncertainty models are gaining increasing importance in engineering sciences, and the intensive research in this field worldwide is a sure sign of wider application in the future (Moller, 2004). Developments so far are outlined in Figure 2.7:

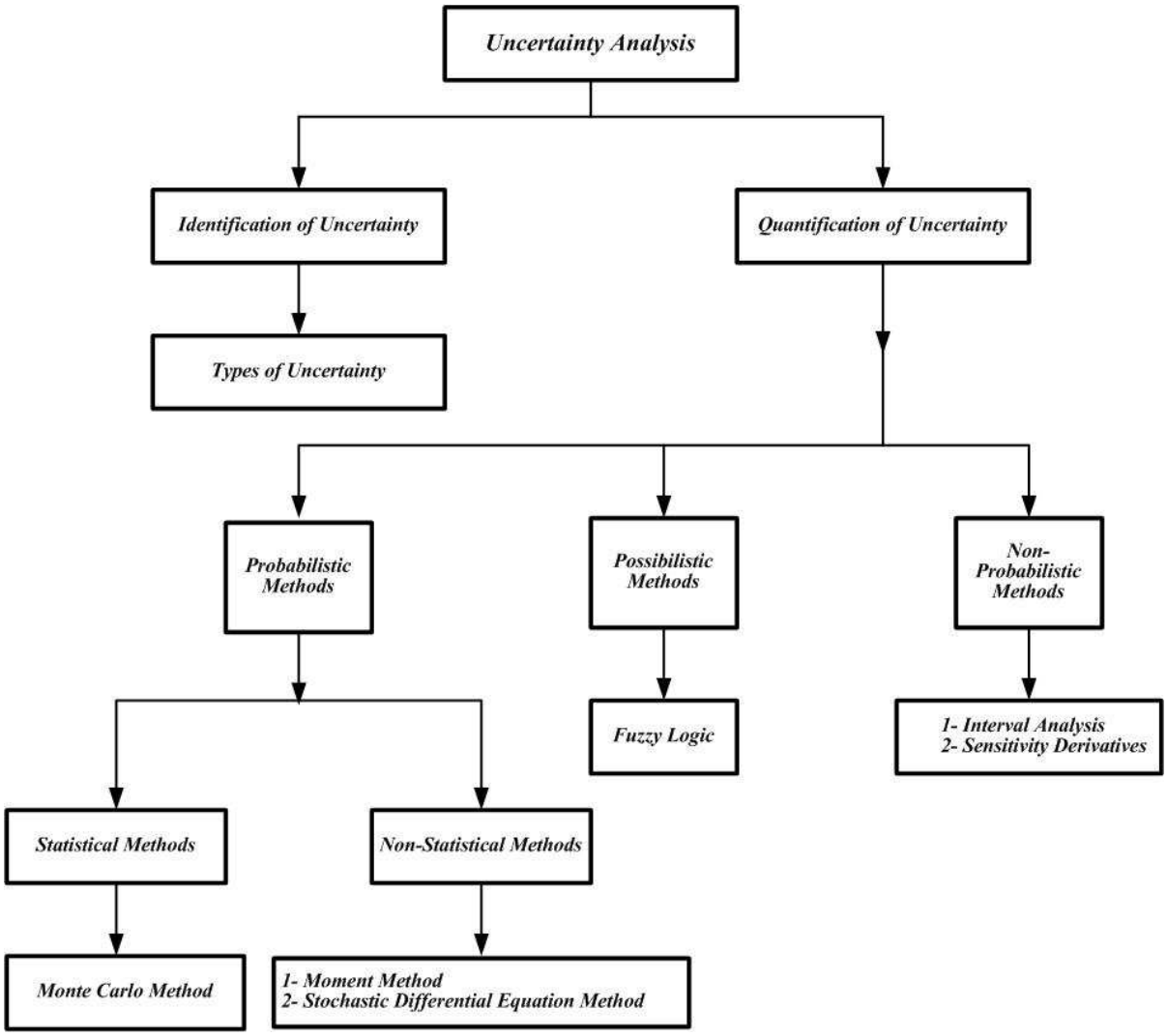

Figure 2.7 Uncertainty Analysis: Identification and Quantification of Uncertainty

2.5.1 Identification of Uncertainty

The first step in uncertainty analysis is to identify all the uncertainties from the analyzed structure and to associate these uncertainties with the different uncertainty types mentioned in the previous section.

2.5.2 Quantification of Uncertainty

The goal of uncertainty quantification is to characterize the effect that different types of uncertainty have on physical experiment or numerical simulation output. Traditionally, there are different classes of uncertainty analysis methods corresponding to different ways of characterizing the uncertainty in the input variables. These methods will be discussed in the following sections.

2.5.2-1 Probabilistic Methods

Probabilistic methods can be divided into "statistical" and "non-statistical" methods. Statistical methods use a large number of values of the input variables to calculate values repeatedly for the output variables. A sampling method is used to generate the input values from a distribution. Statistics, such as the mean and variance, of the output values can then be calculated.

Non-statistical methods use an analytical treatment of the uncertainty. Two examples of these methods are the "moment" methods and "stochastic differential equation" (SDE) methods, which will be discussed later.

A) Statistical methods

Basic Monte Carlo Method:

Monte Carlo methods, which are also called "statistical simulation methods", can be loosely defined to include any method that utilizes sequences of random numbers to perform the simulation. Although they have been used for hundreds of years, the name "Monte Carlo" was given to these methods in 1944 by the group of elite mathematicians and physicists who

were responsible for developing both the first atomic bomb and the first electronic digital computers (Faragher, 2004).

The procedure for the basic Monte Carlo method involves three steps:

1. For each input variable, a set of values is generated by randomly sampling the known or assumed probability density function.

2. For each set of random input data a deterministic mathematical model is executed and the output data are aggregated.

3. The statistics of the output data set (mean, variance, skewness, kurtosis, etc.) are used to define its probability density function

It is important to note that while the Monte Carlo method converges to the exact stochastic solution as the number of samples approaches infinity, the convergence of the mean value estimate is slow because the standard deviation of the mean scales inversely with the square root of the number of samples (Faragher, 2004). Hence thousands or millions of data samples may be required to get the required accuracy, and for each sample the deterministic mathematical model used in step 2 will need to be executed.

The basic Monte Carlo method is very computationally expensive. To reduce the computational expense, modifications of the basic Monte Carlo method have been developed. Two of the modified Monte Carlo methods are called "Importance sampling" and "Latin Hypercube Sampling". They are popular because they are easy to implement and reduce the computation time while still providing the required accuracy in the particular situations described below.

Importance Sampling Monte Carlo Method:

Importance Sampling is one of the variance-reducing modifications to the Monte Carlo method. The fundamental idea is that the sampling process is deliberately distorted or biased (Faragher, 2004). Instead of taking samples at random from a PDF, a "sampling PDF" is designed to take more samples from a region of importance. Importance sampling is particularly valuable because the largest gains are possible in some of the most difficult simulation applications, those involving the simulation of rare events. A sampling distribution designed to take more samples in the region where events are rare reduces the number of simulations required to observe an adequate number of such events.

Reduction in computation time of many orders of magnitude is possible by using Importance Sampling instead of the basic Monte Carlo method with the same accuracy when rare events are involved (Faragher, 2004). Unfortunately, in applications that do not involve rare events the design of the sampling distribution can be very difficult with the result that the Importance Sampling method may increase the simulation time or fail.

Latin Hypercube Monte Carlo Method:

In the Latin Hypercube sampling method the selection of sample points is highly constrained (Faragher, 2004). This enables the statistics of the sample (mean, variance, etc.) to resemble the statistics of the probability density function (PDF) being sampled with the same accuracy for a smaller sample size than is required for the basic Monte Carlo sampling method. For a single uncertain input parameter, instead of taking N samples at random from the complete PDF, the range of probable values is partitioned into N segments of equal probability. That is, each segment corresponds to an equal area under the PDF curve.

The advantage of the Latin Hypercube sampling method is that the random samples are generated from all the ranges of possible values. While this method ensures complete coverage of the full range of the input parameters it does not give accurate information about the tails of the output probability density functions.

Response Surface Monte Carlo Method:

Pratt & Whitney Inc. developed a probabilistic design system incorporating two different methods depending on whether or not the computer codes being used were computationally expensive to run (Faragher, 2004). For the codes that could be run quickly they used the Monte Carlo method of randomly varying the inputs and calculating the mean and variance of the calculated outputs. For codes that run slower, they used a second order response surface model with Box-Behnken design experiments, followed by a Monte Carlo simulation. The Box-Behnken design experiments use just three values of each uncertain input variable: low, nominal and high. With six variables the Box-Behnken design means the computer code has to be run only 49 times. A second order response surface regression equation is then fitted to the output variables from the 49 runs. A Monte Carlo simulation is simply performed by selecting a random sample value of each input variable according to its PDF, and then calculating the corresponding output values from the response surface equation. Several thousand Monte Carlo samples can be evaluated in a very short time.

Random Number Generators for Monte Carlo Simulations:

Generating "good" random numbers can be a major problem in Monte Carlo Simulations. Many basic random number generators (RNGs) supplied with computers are not sufficiently random. Even some RNGs with adequate randomness properties are not good enough for Monte Carlo simulation because their period of repetition is too small. The period

must be much greater than the number of random numbers used in the simulation, or else the results can be incorrect.

Multiplicative linear congruential generators (MLCG) using 32-bit integers have a period of at most $2^{31} \cong 10^{10}$ (Faragher, 2004). This many random numbers can be generated in a matter of seconds on a modern workstation.

B) Non-Statistical methods

Moment Methods:

The moments of a probability distribution are its defining features.

- The first moment is the mean
- The second moment is the variance
- The third moment is the skewness
- The fourth moment is the kurtosis (peakiness)

A normal or Gaussian probability distribution is completely defined by its first two moments, its mean and variance. Other types of probability distribution are not so simple. Moment methods ignore the higher order moments and approximate the probability density functions, which characterize the uncertainty in the input parameters by their first two moments (Faragher, 2004).

Moment methods are very simple, convenient and widely used approximate methods for estimating the moments of the output from the moments of the uncertain input parameters (Faragher, 2004). These methods are also called perturbation methods. These methods involve some form of perturbation expansion in terms of random variables present in the

problem, taken about a deterministic state (often the one corresponding to the mean value of these random variables). Among these, the first-order second moment method is based on the truncation of the Taylor-series expansion of the random quantities after the terms involving first-order partial derivatives with respect to the random variables in the problem.

Stochastic Differential Equation Methods:

Stochastic Differential Equation (SDE) methods have been used for structural mechanics problems (Faragher, 2004). They provide the information about the higher moments of the results at less computational expense than Monte Carlo methods.

2.5.2-2 Non-Probabilistic Methods

A) Interval Analysis:

In interval analysis, a pair of numbers representing the maximum and minimum values that the variable is expected to take replaces the value of a variable. Interval arithmetic rules are then used to perform mathematical operations with the interval numbers (Faragher, 2004). While interval analysis has been applied successfully to small problems, it has not found practical application to large simulations because the results it produces are too conservative, i.e. it predicts the greatest possible uncertainty in the output. Also, its ease of implementation is out-weighed by the lack of information it provides compared with other methods.

B) Sensitivity Derivatives:

This deterministic technique has been in use for many years. Its aim is to quantify the sensitivity of the output to a variation in one of the inputs. In this way the total uncertainty in the output is divided between the various sources of uncertainty. It identifies which sources

of uncertainty have a significant effect on the output and which sources can be ignored (Faragher, 2004). As such, it is often a useful preliminary step performed before a computationally expensive probabilistic uncertainty analysis.

2.5.2-3 Possibilistic Methods - Fuzzy Logic

Fuzzy logic can be used to estimate the uncertainty in the output when the uncertainties of the input parameters are characterized by membership functions. Fuzzy logic calculates approximate behavior of the system using models based on inexact, incomplete, or unreliable data. The membership function represents the degree of membership of the fuzzy variable within a fuzzy set. Uncertainty analysis using membership functions is sometimes referred to as "possibilistic", to contrast this approach with the probabilistic approach using probability density functions to characterize the uncertainty in the input parameters. More information about this technique can be found in (Faragher, 2004). Although fuzzy logic is appealing because of its simplicity, many aerospace applications require a high level of accuracy that makes it necessary to employ probabilistic methods wherever it is possible to do so.

2.6 Conclusions about Quantification of Uncertainty

The basic Monte Carlo method provides the complete information about the higher statistical moments of the results but it is very computationally expensive. In order to reduce this expense modified Monte Carlo methods such as Latin Hypercube Sampling or Importance Sampling have been developed.

Moment methods are popular because of their low computational expense. They will not give good results unless the probability distribution of the uncertainty in the input parameters is close to Gaussian because they ignore the higher order moments.

Stochastic Differential Equation methods provide the complete information about the higher statistical moments at less computational expense than Monte Carlo methods. Therefore, if this information is needed, and if the approximation involved in the response surface Monte Carlo method is not acceptable, the SDE methods are the best alternative (Faragher, 2004).

Non-probabilistic methods are often a useful preliminary step performed before a computationally expensive probabilistic uncertainty analysis. Also, its ease of implementation is out-weighed by the lack of information it provides compared with other methods.

Although possibilistic methods are appealing because of its simplicity, many aerospace applications require a high level of accuracy that makes it necessary to employ probabilistic methods wherever it is possible to do so.

2.7 Probabilistic Structural Health Monitoring using the Monte Carlo Simulation.

Due to the unavoidable uncertainties that are presented in the physical models and the parameters, and etc, the probabilistic framework is a tool very well suited to handle the SHM problem. Probabilistic method considering the uncertainty issue is presented in this work. A measure of the confidence level of the damage location is examined by taking uncertainties into account.

The probabilistic structural health monitoring procedure is explained in the following steps:

Firstly, an elastic wave energy decay model for wave propagating in plates is established. The physical model imposes assumptions and simplifications. This model uncertainty is modeled as a PDF.

Secondly, the stochastic uncertainty due to the presence and change of environments is modeled as a PDF.

Thirdly, the least-squares method in conjunction with the Monte Carlo simulation for each uncertainty and its interaction is applied to iteratively search localized damage based on elastic wave energy measurements.

Lastly, a probabilistic diagram for the location of the damage can be constructed using the moments (mean, variance, etc) of the resulting PDF of the damage location.

In the mathematical equations, the location of the damage is a nonlinear function of the measured sensor data and the physical model. Since, the measured sensor data and the physical model are represented as a PDF, the location of the damage is a PDF as well. In order to generate the random numbers from a Gaussian PDF and to solve for the resultant PDF of the damage location, the Monte Carlo simulation is used.

2.8 Development of the Elastic Wave Energy Decay Model, Measurements, and the Model Parameters.

In order to obtain the reflected waves solely from damages, the response wave signal at each sensor is measured before and after damage occurred. The pre-damage wave signals

are subtracted from the post-damage wave signals. Let M be the number of sensors, N be the data length collected by each sensor and only one damage exits in the plate. Figure 2.8 shows the scheme of sensor and actuator deployment with the damage location.

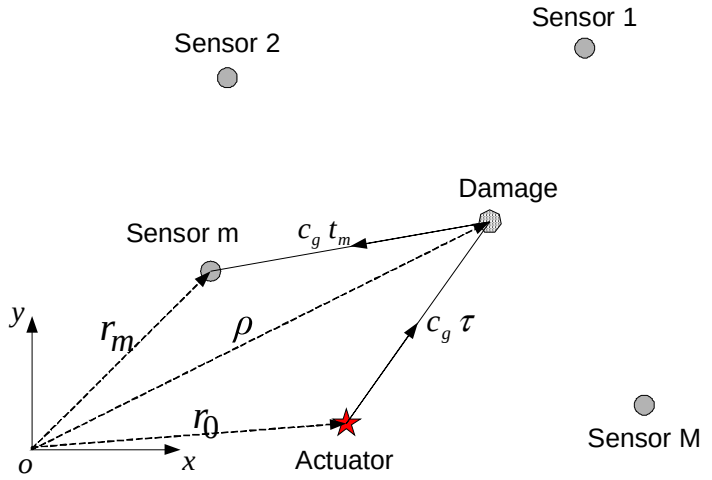

Figure 2.8 Scheme of sensor/actuator deployment and unknown damage

The signal received by each sensor can be modeled as (Yang and Yuan, 2005):

$$x_m(n) = \gamma_m \frac{\alpha\, a_0(n - t_m - \tau)}{\left\| \boldsymbol{\rho} - \boldsymbol{r}_m \right\|}, \quad m = 1, 2, \cdots, M\ ,\ n = 1, 2, \cdots, N \tag{2.8-1}$$

where $x_m(n)$: the n^{th} value sampled at the m^{th} sensor over time interval $1/\ f_s$;

f_s is the sampling rate;

γ_m: Sensor gain factor of the m^{th} sensor;

$\boldsymbol{\rho}$: The position vector of the damage;

$\boldsymbol{r}_m$: Cartesian coordinates of the sensor m;

α: Reflection factor or the initial amplitude at the damage;

$a_0(n - t_m - \tau)$: Normalized reflected waveform from damage with unit peak-to-peak value;

t_m : Time delay from the damage to sensor *m*;

τ : Time delay from the actuator to the damage.

$$t_m = \frac{f_s \|\boldsymbol{\rho} - \mathbf{r}_m\|}{c_g} \text{ and } \tau = \frac{f_s \|\boldsymbol{\rho} - \mathbf{r}_0\|}{c_g} \tag{2.8-2}$$

where $\boldsymbol{r}_0$ is a given vector denoting Cartesian coordinates of the actuator, c_g indicates the group velocity and the operator $\| \ \|$ indicates Euclidean distance. It is worth of noting that multiplying f_s in Eq. (2.8-2) is because of the discrete time consideration.

The excitation is a Hanning windowed sinusoid burst signal governed by the following function:

$$q(t) = P[H(t) - H(t - N_p / f_c)] \times [1 - \cos(2\pi f_c t / N_p)] \sin(2\pi f_c t) \tag{2.8-3}$$

where $H(t)$ is the Heaviside step function, N_p is the number of peaks of the loading and f_c is the central frequency. In this study, $N_p = 5$, and $f_c = 50\text{kHz}$ are used.

The reflected waveform also has the same shape as Eq (2.8-1), thus we have $a_0(t) = [H(t) - H(t - N_p / f_c)] \times [1 - \cos(2\pi f_0 t / N_p)] \sin(2\pi f_0 t)$ and the expectation of $a_0(n)$, or even its delay, equals to zeros if *N* is large enough.

$$\mathrm{E}[a_0(n)] = 0, \quad \mathrm{E}[a_0(n - t_{km} - \tau_k)] = 0 \tag{2.8-4}$$

The expectation of energy is calculated by averaging over a time window $T = N / f_s$. Denoting the scalar $\mathrm{E}[x_{\mathrm{m}}^2(n)]$ as y_m, the energy decay model can be expressed as:

$$\hat{y}_m = \mathrm{E}[x_m^2(n)] = \frac{1}{N} \sum_{n=1}^{N} x_m^2(n) = \frac{g_m}{N} \sum_{n=1}^{N} \left[\frac{\alpha a_0(n - t_m - \tau)}{\|\boldsymbol{\rho} - \mathbf{r}_m\|} \right]^2 \tag{2.8-5}$$

where $g_m = \gamma_m^2$ and note that $a_0(n - t_m - \tau)$ is a $N \times 1$ vector.

In practice, $\hat{y}_m$ is the modeled energy which estimates the reflected wave signals, furthermore, the corresponding measurement is $\hat{y}_m$ may be viewed as the extracted characteristic from the collected data at the m^{th} sensor.

In Eq. (2.8-5), we have two unknown variables of the damage location coordinates and one unknown damage reflection factor α, that is, the three unknown parameters are defined as

$$\theta = \{\rho_x \quad \rho_y \quad \alpha\} \tag{2.8-6}$$

Since there are totally three unknown variables, there must be at least three or more sensors reporting wave energy measurements to yield a solution.

2.9 Development of the Probabilistic SHM using the Monte Carlo Simulation

To obtain the physical model that reflects the true behavior of the real model, several assumptions were made. These assumptions are shown below:

1) Since the isotropic aluminum plate is tested, group velocity is independent of wave propagation direction because the isotropic aluminum plate is tested.

2) The size of incipient damage is relatively small so that reflected waves from the damage can be treated as a secondary wave point source.

3) Excitation wave signals are narrow banded and their central frequencies are lower than the cut-off frequency. Thus the dispersion effect is largely neglected. All the excitation wave signals are dominated by the A_0 mode.

Due to the last assumption and the strength of the signal being inversely proportional to the distance between damage and the sensor, an uncertainty in the physical model arises. A Gaussian distribution function is used to model the uncertainties in modeled reflected signal:

$$\mathbf{a}_0 = \frac{1}{\sigma_{a_0}\sqrt{2\pi}} e^{-\frac{(a_0-\mu_{a_0})^2}{2\sigma_{a_0}^2}} \tag{2.9-1}$$

where μ_{a_0} is the mean and σ_{a_0} is the standard deviation.

The measured data y_m will be also modeled as a Gaussian distribution with a mean and a variance. This data will be treated as uncertain data and this is due to the fact that during the experiment, changes in the environmental conditions such as temperature and humidity as well as the inaccuracy of the equipments used will result in such an uncertainty. Therefore, the PDF of y_m is:

$$\mathbf{Y}_m = \frac{1}{\sigma_{y_m}\sqrt{2\pi}} e^{-\frac{(y_m-\mu_{y_m})^2}{2\sigma_{y_m}^2}} \tag{2.9-2}$$

In the mathematical model given in Eq. (2.8-5), the distribution of the parameters, $\theta = \{\rho_x \quad \rho_y \quad \alpha\}$, will be modeled as Gaussian PDFs.

These parameters are modeled as a Gaussian distribution function with an initial mean and variance:

$$\mathbf{P}_x = \frac{1}{\sigma_x\sqrt{2\pi}} e^{-\frac{(\rho_x-\mu_x)^2}{2\sigma_x^2}} \tag{2.9-3}$$

$$\mathbf{P}_y = \frac{1}{\sigma_y\sqrt{2\pi}} e^{-\frac{(\rho_y-\mu_y)^2}{2\sigma_y^2}} \tag{2.9-4}$$

$$\alpha = \frac{1}{\sigma_\alpha \sqrt{2\pi}} e^{-\frac{(\alpha-\mu_\alpha)^2}{2\sigma_\alpha^2}} \tag{2.9-5}$$

In order to conclude the different types of uncertainties included in this work, Figure 2.9 is developed:

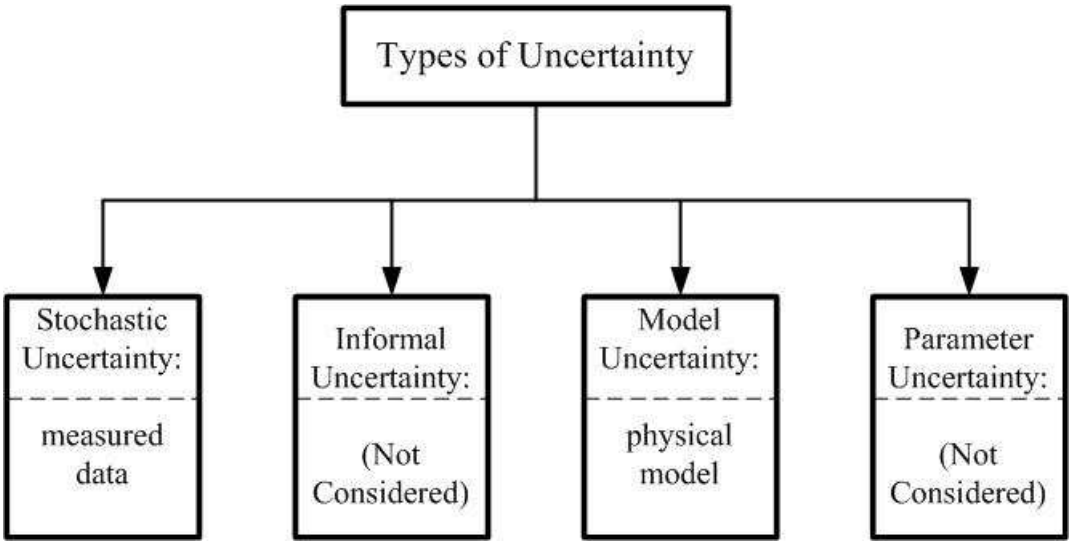

Figure 2.9 Uncertainties included in this work

Due to the different uncertain variables mentioned before, Monte Carlo simulation is used. The Monte Carlo simulation is an engineering tool that enables us to perform probabilistic analysis when many uncertain variables are related through non-linear equations. The Monte Carlo method is used to determine the resultant PDF of the damage location, which is dependant on the PDFs of the model uncertainty and the measurement uncertainty. This procedure is represented in Figure 2.10.

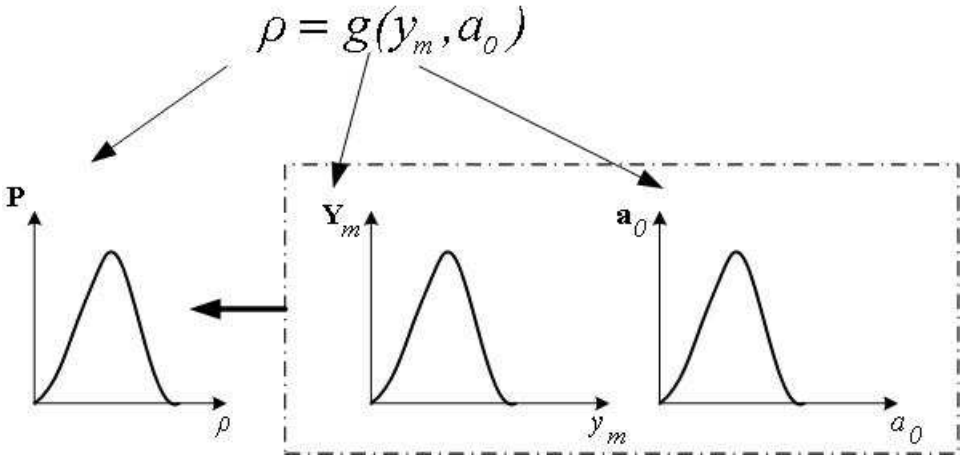

Figure 2.10 Graphic representation of the problem of the probabilistic analysis presented in this work

For each random variable (uncertainty), 5000 samples are generated to model the Gaussian PDF. For each set of random variables, a deterministic mathematical model is executed and the output data are aggregated.

The mathematical model of the wave energy is:

$$\hat{\mathbf{Y}}_{\mathrm{m}}(\theta) = \frac{g_m}{N} \sum_{\mathrm{n}=1}^{\mathrm{N}} \left[\frac{\boldsymbol{\alpha}\, \boldsymbol{a}_0(n - t_m - \tau)}{\left\| \mathbf{P} - \boldsymbol{r}_{\mathrm{m}} \right\|} \right]^2 \tag{2.9-6}$$

The distribution function $\hat{\mathbf{Y}}_{\mathrm{m}}(\theta)$ is obtained using the Monte Carlo method as well.

In this thesis, a least-squares method uses the energy measurement of the collected elastic wave signals such that it uses all the data information including the time-of-flight. Furthermore, since the least-squares method is based on active diagnostic technique to obtain the reflection waves, it is a promising method for the application of SHM.

In the least-squares method, the PDF of the parameters $\theta = \{\rho_x \quad \rho_y \quad \alpha\}$ are iteratively updated to make the following error function between the mean of the PDF of the modeled record and the mean of the PDF of the measured data reach its minimum:

$$\mathbf{J}(\theta) = \frac{1}{2}\sum_{m=1}^{M}[\text{mean}(\mathbf{Y}_m) - \text{mean}(\hat{\mathbf{Y}}_m(\theta))]^2 \tag{2.9-7}$$

where $\hat{\mathbf{Y}}_m(\theta)$ is the PDF for the modeled wave energy and $\mathbf{Y}_m$ is the PDF for the measured wave energy at sensor *m*, respectively.

$\mathbf{J}(\theta)$ is then represented as a PDF as well using the Monte Carlo method:

$$\mathbf{J}(\theta) = \frac{1}{2}\sum_{m=1}^{M}[\mathbf{Y}_m - \hat{\mathbf{Y}}_m(\theta)]^2 \tag{2.9-8}$$

The gradient of $\mathbf{J}(\theta)$ with respect to $\boldsymbol{\alpha}$ is

$$\frac{\partial \mathbf{J}(\theta)}{\partial \boldsymbol{\alpha}} = 2\boldsymbol{\alpha}\sum_{m=1}^{M} g_m(\mathbf{Y}_m - \hat{\mathbf{Y}}_m(\theta))\frac{1}{N}\sum_{n=1}^{N}\frac{\boldsymbol{a}_0^2(n - t_m - \tau)}{\left\|\mathbf{P} - \boldsymbol{r}_m\right\|^2} \tag{2.9-9}$$

The gradient of $\mathbf{J}(\theta)$ with respect to the p^{th} component of the PDF of the damage coordinates $\boldsymbol{\rho}$ can be expressed as

$$\frac{\partial \mathbf{J}(\theta)}{\partial \mathbf{P}_{.p}} = 2\boldsymbol{\alpha}^2\sum_{m=1}^{M} g_m(\mathbf{Y}_m - \hat{\mathbf{Y}}_m(\theta))\frac{1}{N}\sum_{n=1}^{N}\left[\frac{(\boldsymbol{r}_{mp} - \mathbf{P}_{.p})\boldsymbol{a}_0^2(n - t_m - \tau)}{\left\|\mathbf{P} - \boldsymbol{r}_m\right\|^4}\right. \tag{2.9-10}$$

$$\left. + \frac{2f_s}{c_g}\frac{\boldsymbol{a}_0(n - t_m - \tau)\ \boldsymbol{a}_0'(n - t_m - \tau)}{\left\|\mathbf{P} - \mathbf{r}_m\right\|^2}\cdot\left(\frac{\boldsymbol{r}_{mp} - \mathbf{P}_{.p}}{\left\|\mathbf{P} - \boldsymbol{r}_m\right\|} + \frac{\boldsymbol{r}_{0p} - \mathbf{P}_{.p}}{\left\|\mathbf{P} - \boldsymbol{r}_0\right\|}\right)\right]$$

where the subscript *.p* denotes the p^{th} component of coordinates and sub-prime is the derivative with respect to its argument.

The above procedure leads to a so-called Gradient optimization algorithm:

Gradient optimization algorithm

Initialization:

Initial mean and variance values for damage positions $\{\boldsymbol{\rho}\}$ *and damage reflection factors* α

Initialize mean and variance values for $\mathbf{Y}_m$

Initialize mean and variance values for the model uncertainty

After initialization, $\frac{\partial \mathbf{J}(\theta)}{\partial \boldsymbol{\alpha}}$ and $\frac{\partial \mathbf{J}(\theta)}{\partial \mathbf{P}_{.p}}$ will be calculated.

Then for the next iteration the PDFs will be updated as

$$\mathrm{f}(\boldsymbol{\alpha})^{(\mathrm{i}+1)} = \mathrm{f}(\boldsymbol{\alpha})^{(\mathrm{i})} - \varsigma_1 \frac{\partial \mathbf{J}(\theta)}{\partial \boldsymbol{\alpha}} \tag{2.9-11}$$

$$\mathrm{f}(\mathbf{P}_{.p})^{(\mathrm{i}+1)} = \mathrm{f}(\mathbf{P}_{.p})^{(\mathrm{i})} - \varsigma_2 \frac{\partial \mathbf{J}(\theta)}{\partial \mathbf{P}_{.p}} \tag{2.9-12}$$

where ς_1 and ς_2 are positive scalars called step size.

Repeat until convergence

Calculate Eq. (2.9-9) and Eq. (2.9-10)

Update Eq. (2.9-11) and Eq. (2.9-11)

The convergence criterion is given by

$$\left\| \mathrm{mean}(\mathbf{P}_{.p}^{(\mathrm{i}+1)}) - \mathrm{mean}(\mathbf{P}_{.p}^{(\mathrm{i})}) \right\| \leq 0.0001 \tag{2.9-13}$$

In order to find the probability of the damage location in a certain area, the joint distribution function of $\mathbf{P}_x$ and $\mathbf{P}_y$ is calculated. The theoretical development in Section 2.3 has been used to calculate the probability of the damage within a certain area. The plate is divided into grids of size 0.5 cm along the *x*-axis and 0.5 cm along the *y*-axis. This results in 14400 rectangular areas (See the Figure below).

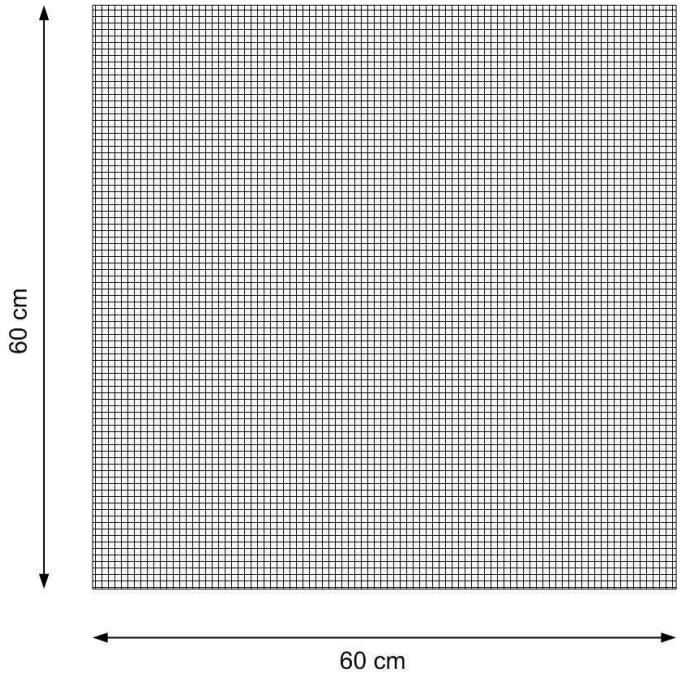

Using Eq. (2.3.7), the probability of the damage being within every single area $(0.25 cm^2)$ is found. The analysis is performed by taking the 5000 coordinates from the resultant PDF of **P** and calculating the probability of every single point to fall within every area.

As a conclusion, the idea of the Monte Carlo technique is to randomly pick values from the uncertain parameters and the uncertain measured and modeled data such that the histogram of the chosen values approximates a PDF. The Monte Carlo process consists of sampling the uncertain parameter and the uncertain data values from the assumed uncertainty distributions and running the simulation code for each set of values. This procedure of the identification of uncertainty can therefore be viewed as nothing more than a multiple runs of a deterministic computer program.

3 Simulation and Experimental Results

3.1 Simulation Results and Discussion

The simulation results of a single damage localization based on the probabilistic least-squares method are illustrated as follows. The aluminum plate (A1-6061) used in this study and its material properties are listed in Table 3.1. The central frequency of the excitation signal is set at 50 kHz, which is less than the first cut-off frequency such that only the lowest flexural wave exists. The group velocity c_g corresponding to 50 kHz is 2107 m/s.

E (GPa)	ν	ρ (kg/m^3)	h (cm)	Dimension (cm×cm)
72.0	0.3	2730	0.32	152.4×152.4

Table 3.1 Material properties and geometry of Al-6061 plate

In order to generate the simulated wave signal received by each sensor, a finite difference algorithm based on Mindlin Plate theory is used to synthesize the waves in the aluminum plate (Lin and Yuan, 2001). A 600×600 finite difference mesh is with uniform square grid space $\Delta x = \Delta y = 2.54\,mm$ superimposed on the plate region. The thickness of the plate is 0.32 cm. The origin of the coordinate system is set at the center of the plate. A damage is modeled located at (20,10) cm. The point damage is modeled as a material with $1/16$ the value of the bending stiffness for the undamaged plate. In addition, four sensors are located at (-30, 30) cm, (30, -30) cm, (30, 30) cm and (-30, -30) cm. The parameters of the excitation signal are set as $N_p = 5$, and $f_c = 50kHz$. Note that the origin of the coordinate system is at (0,0). Figure 3.1 displays the simulated damage reflected wave signals received at four sensors by using the finite difference algorithm.

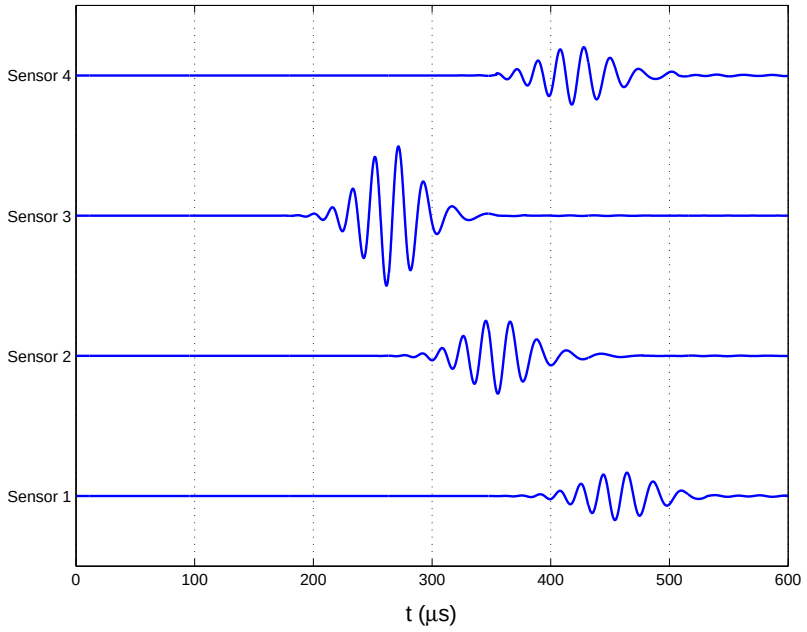

Figure 3.1 Simulated reflected wave packs from the damage using finite difference method

The influence of the level of uncertainty on the resulting PDF of the damage location is studied. Changing the standard deviation of the PDF changes the level of uncertainty. A standard deviation that is equal to 0.1 (or 10% of uncertainty) demonstrates a low level of uncertainty, whereas a standard deviation that is equal to 1 demonstrates a high level of uncertainty (Vanik, 1997). Several simulations are developed to study the effect of changing the level of uncertainty on detecting the damage location.

In order to detect a single damage locating at (20, 10) cm, the minimum number of sensors that should be used is three (Wang, 2004). Figure 3.2 shows the final localization results and the performance of searching for the four-sensor setup. Compared with three sensors case, the searching procedure will speed up remarkably when four sensors are used. However, more sensors may also add up the computational cost of the optimization algorithm. There is a trade-off between the numbers of sensors and computational cost.

Generally the former effect is dominant, thus the number of sensors should be somewhat larger than the necessary number of sensor in the application of real -time damage detection.

Figure 3.2 shows a plot of the different searching traces with different initial guess positions. This figure shows the result of zero level of uncertainty. Zero level of uncertainty corresponds to a deterministic method that is used as a base for estimating the damage location with different degrees of uncertainties. The targeted damage location is at (20, 10) cm. The method converges to a damage position (18.4, 10.2) cm, which makes the difference between the actual damage location and the estimated damage location to be 1.6 cm. From this result, it can be seen that this method has a robust performance and good convergence.

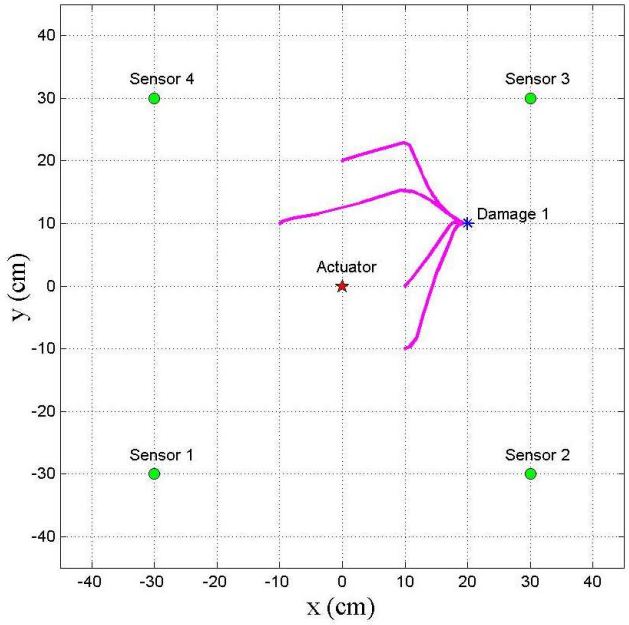

Figure 3.2 Simulation results of damage localization by least-squares method

In order to study the sensitivity of the damage localization to the stochastic and model uncertainty, different levels of model and stochastic uncertainties are analyzed. Figures 3.3, 3.4 and 3.5 show the probability distribution, the histograms and the PDFs for different levels of model uncertainty and zero stochastic uncertainty. From the mean of the PDFs, it can be

noticed that the estimated damage location with 5%, 10% and 20% model uncertainty is respectively at (18.4, 10.3) cm, (18.3, 10.3) cm and (18.3, 10.6) cm., which is very close to the damage location obtained from the deterministic analysis. Thus, the mean of the PDFs, which corresponds to the damage location with the highest probability, is not very sensitive to the model uncertainty. In contrast, as the level of the model uncertainty increases, the standard deviation of the PDFs widens. Therefore, increasing the level of the model uncertainty, the damage can be estimated in a wider region (Less confidence level). Consequently, we can conclude in this problem that the model uncertainty affects the standard deviation of the PDF. Therefore, upon increasing the level of the model uncertainty, the standard deviation increases and thus the damage can be estimated with a lower probability (less confidence level).

Figures 3.6, 3.7 and 3.8 show the probability distribution, the histograms and the PDFs for different levels of stochastic uncertainty and zero model uncertainty. From these figures, it can be noticed that the estimated damage with 5% stochastic uncertainty is at (17.5, 9.6) cm. The estimated damage location with 10% and 20% stochastic uncertainty is at (17.1, 9.0) cm and (15.8, 8.1) cm, respectively. From the mean of the PDFs, it can be noticed that as the level of the stochastic uncertainty changes, the mean and the standard deviation of the PDFs change. This shows that the stochastic uncertainty alters the mean and the standard deviation of the resultant PDF. By increasing the level of the stochastic uncertainty, the mean of the PDF is shifting away from the actual value of the location of the damage. In addition, the standard deviation increases as the level of the stochastic uncertainty increases, resulting in a less confidence level about the location of the damage. Consequently, we can conclude that

the damage localization is more sensitive to the stochastic uncertainty than the model uncertainty.

Table 3.2 summarizes the different level of stochastic and model uncertainties that has been used in this analysis as well as the results which show that the damage localization is more sensitive to the stochastic uncertainty than the model uncertainty. In addition, Table 3.2 shows the difference between the estimated damage location with different levels of uncertainty and the actual damage location. From these results, it can be noticed that the as the level of uncertainty increases, this difference increases. Comparing the differences that are caused by the stochastic uncertainty and the model uncertainty, it can be noticed that the difference is much larger for the stochastic uncertainty. This proves that the damage localization is more sensitive to the stochastic uncertainty than the model uncertainty.

	Stochastic Uncertainty	Model Uncertainty	Estimated Damage Location (cm)	Standard Deviation (σ_x, σ_y) (cm)	Difference (cm) between the estimated damage and the actual damage location (20, 10) cm
Level of Uncertainty	0%	5%	(18.4, 10.3)	(0.7, 0.7)	1.6
	0%	10%	(18.3, 10.3)	(1.4, 1.2)	1.7
	0%	20%	(18.3, 10.6)	(2.3, 2.1)	1.8
	5%	0%	(17.5, 9.6)	(0.5, 0.3)	2.6
	10%	0%	(17.1, 9.0)	(1.6, 1.0)	3.1
	20%	0%	(15.8, 8.1)	(2.3, 1.6)	4.6

Table 3.2 Influence of the level of uncertainties on Damage Localization (Simulation Results)

For all different levels of model uncertainty (5%, 10%, 20%), the deviation (of the estimated damage location) from the actual damage location remains small. Therefore, the results are acceptable compared to the dimensions of the plate $152.4 \times 152.4 \times 0.32 cm^3$. The same conclusion holds true for 5% and 10% stochastic uncertainty. For 20% stochastic uncertainty, engineering judgment is needed to draw conclusions about the results.

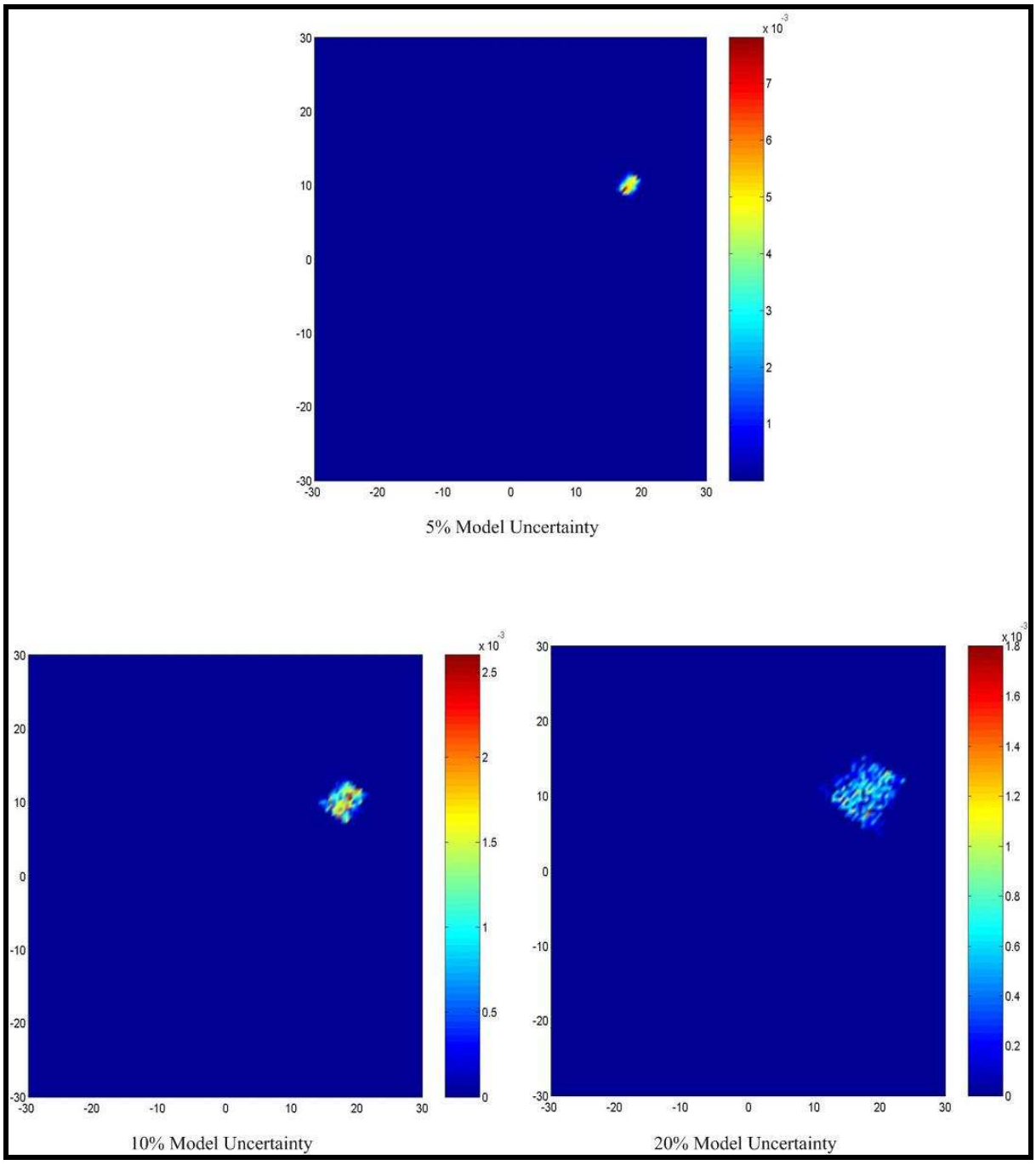

Figure 3.3 Simulation Results: Probability distribution of the damage location with different levels of model uncertainty

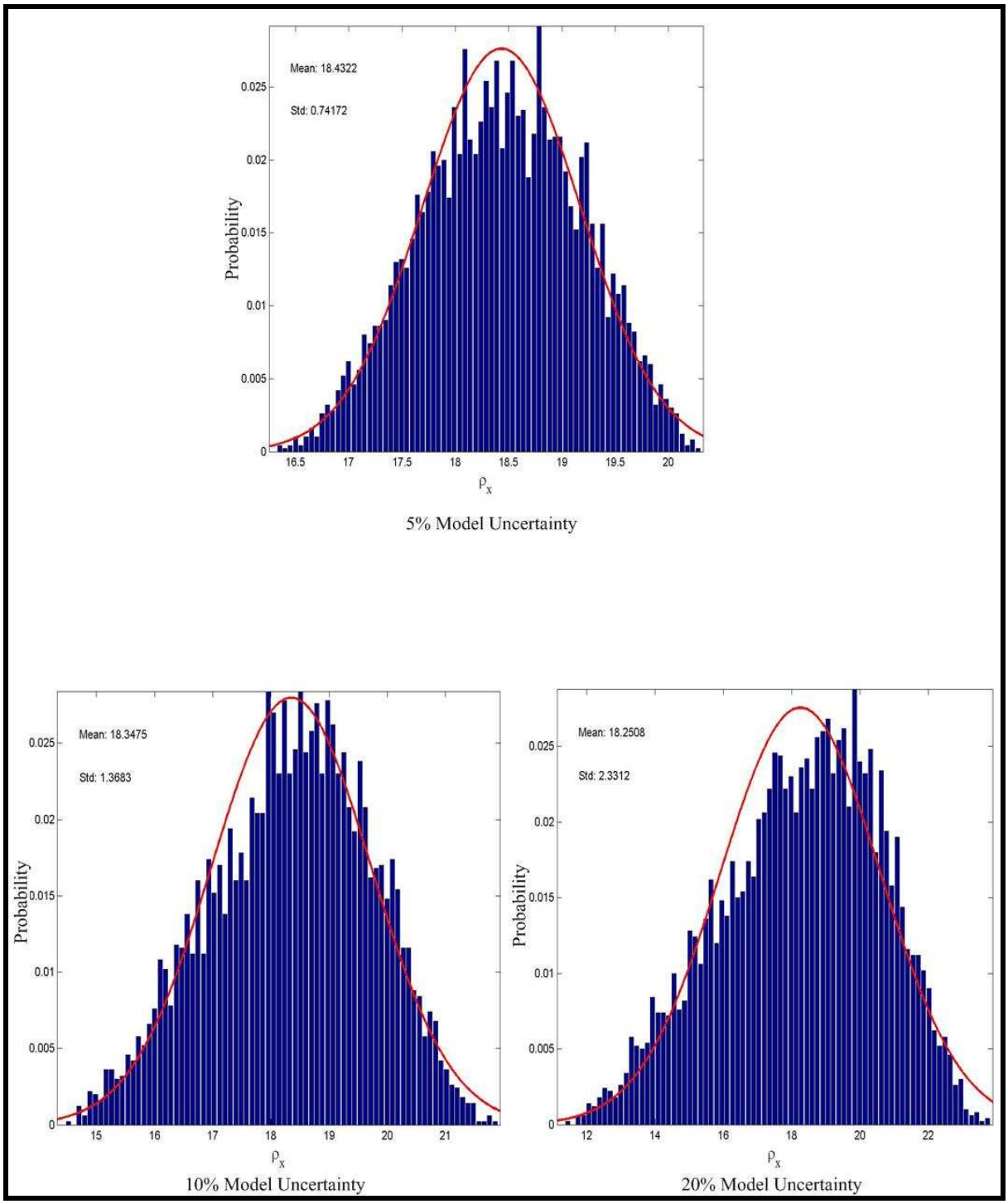

Figure 3.4 Simulation Results: Histograms and the Gaussian probability density functions of ρ_x with different levels of model uncertainty

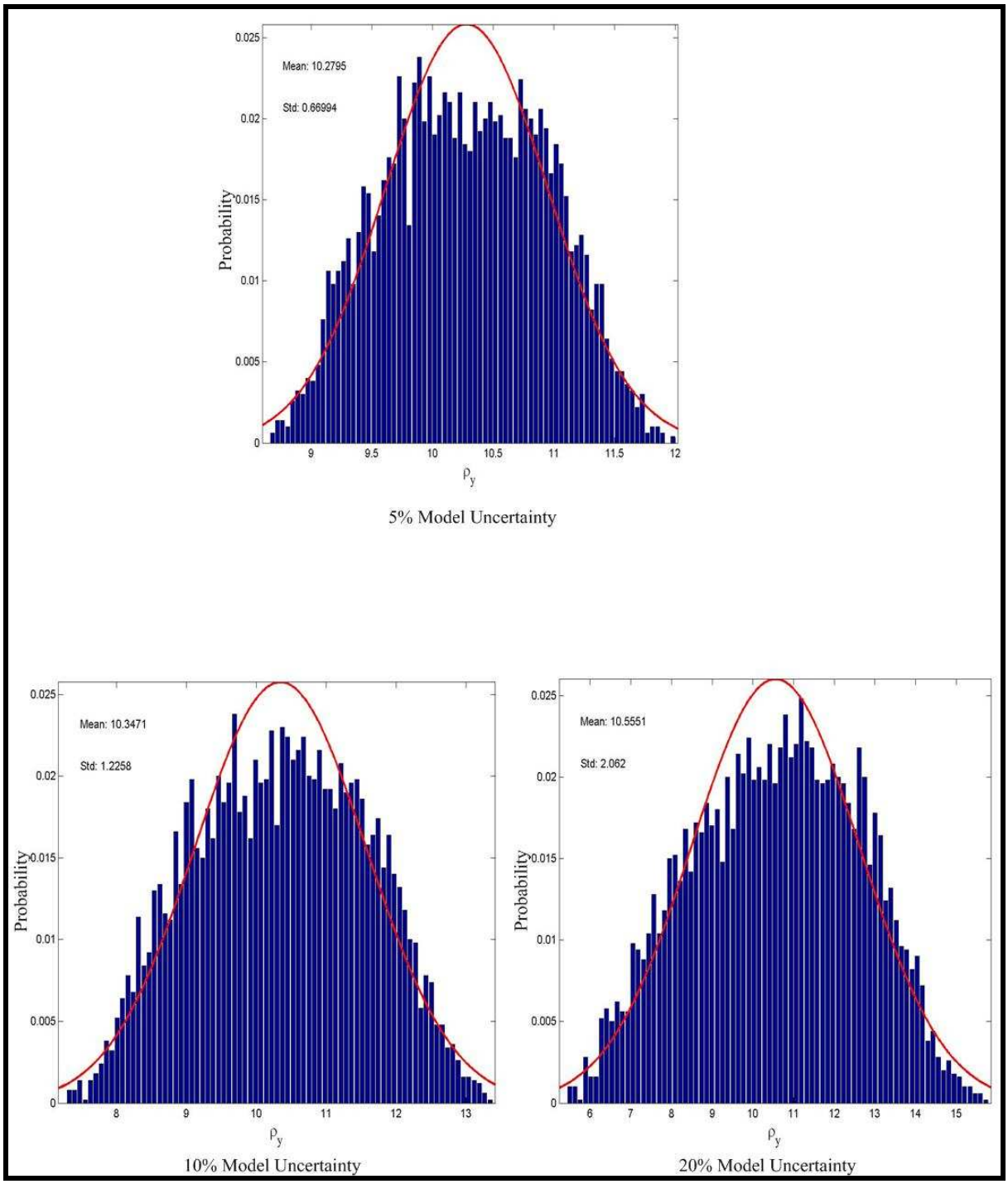

Figure 3.5 Simulation Results: Histograms and the Gaussian probability density functions of ρ_y with different levels of model uncertainty

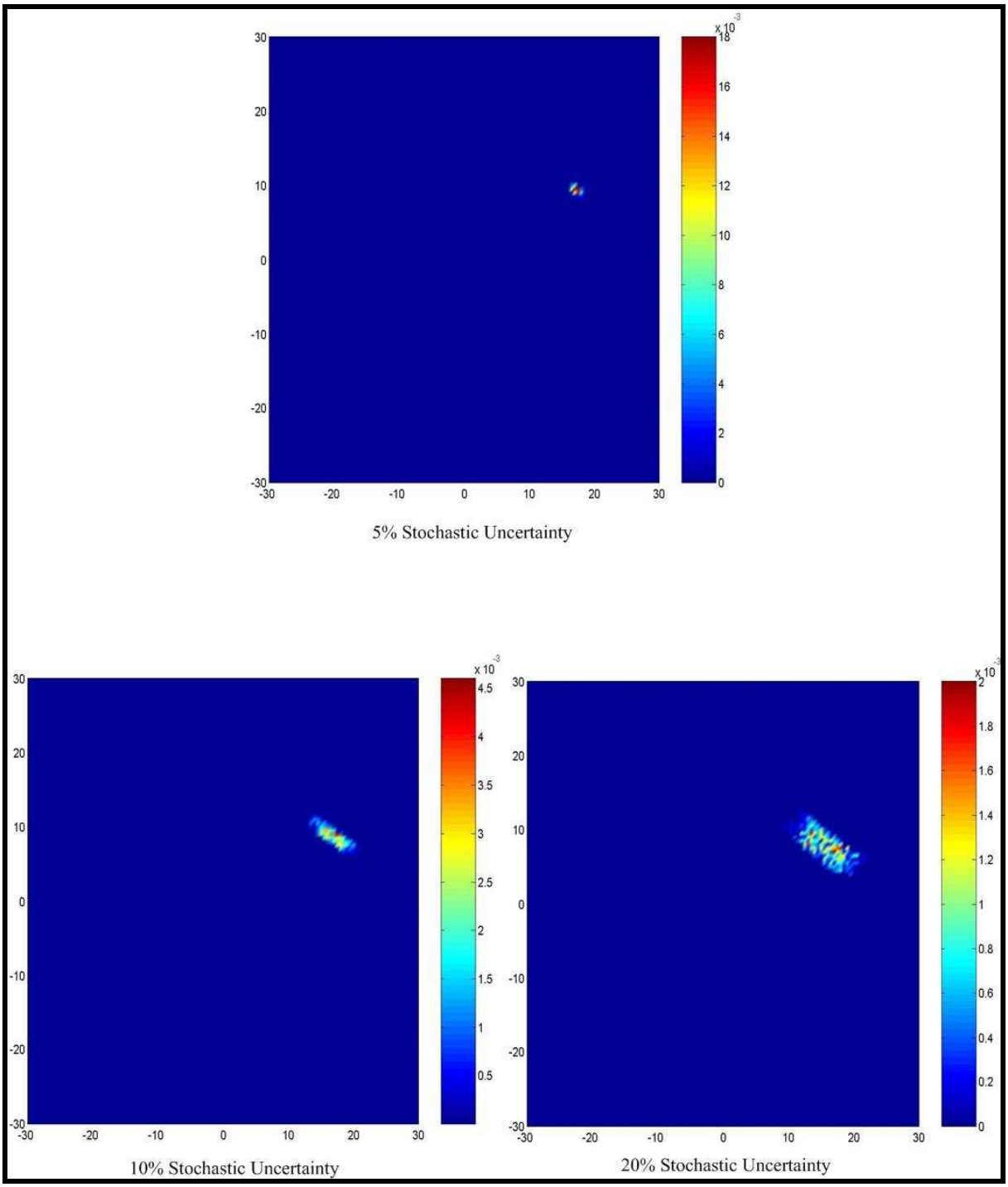

Figure 3.6 Simulation Results: Probability distribution of the damage location with different levels of stochastic uncertainty

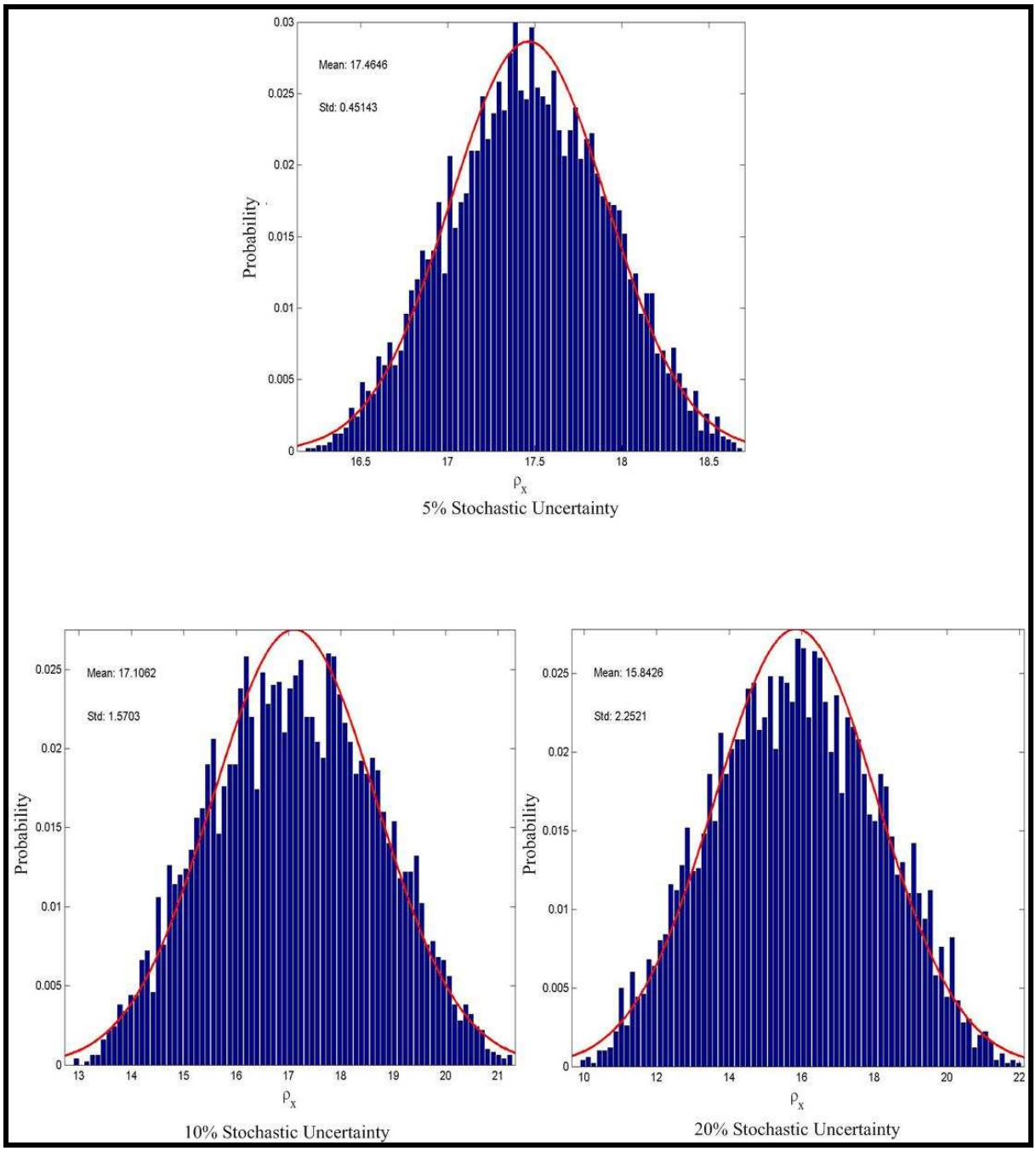

Figure 3.7 Simulation Results: Histograms and the Gaussian probability density functions of ρ_x with different levels of stochastic uncertainty

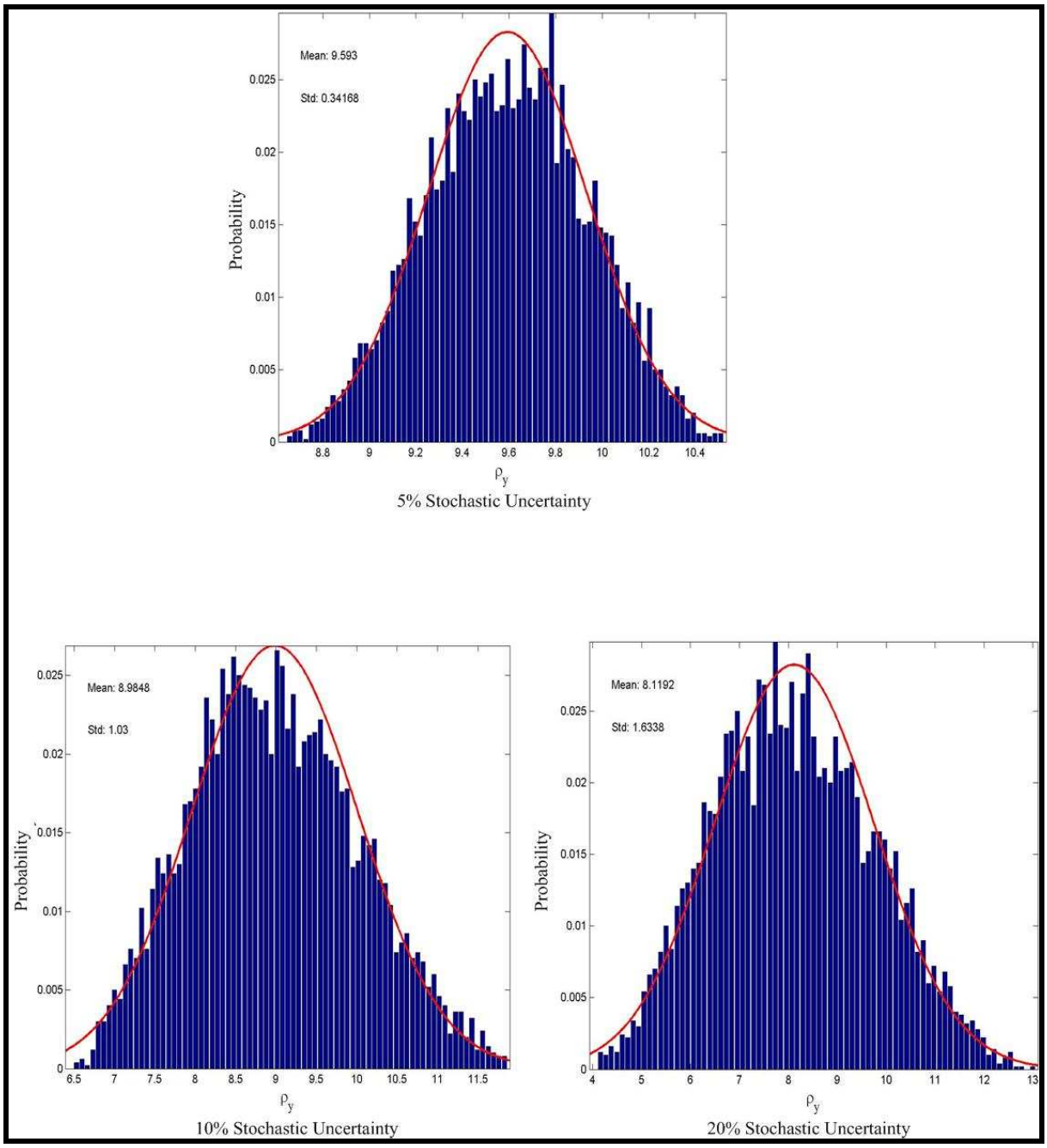

Figure 3.8 Simulation Results: Histograms and the Gaussian probability density functions of ρ_y with different levels of stochastic uncertainty

In the next set of figures, the interaction of model and stochastic uncertainty is studied. Table 3.3 presents different levels of the stochastic and model uncertainty and corresponding results.

	Stochastic Uncertainty	Model Uncertainty	Estimated Damage Location (cm)	Standard Deviation (σ_x, σ_y) (cm)	Difference (cm) between the estimated damage and the actual damage location (20, 10) cm
Level of Uncertainty	10%	5%	(16.9, 9.1)	(2.0, 1.3)	3.3
	5%	10%	(17.5, 9.7)	(1.6, 1.3)	2.5
	20%	10%	(14.9, 8.7)	(4.1, 2.9)	5.3
	10%	20%	(16.5, 9.3)	(3.1, 2.5)	3.5
	20%	20%	(14.9, 8.6)	(3.9, 3.1)	5.3

Table 3.3 Influence of interaction of two different kinds of uncertainty (Simulation Results)

Figure 3.9 through Figure 3.11 show the probability distribution, the histograms and the PDFs for different levels of stochastic and model uncertainty. When the level of stochastic uncertainty is 10% and the model uncertainty is 5%, the estimated damage is at (16.9, 9.1) cm. The deviation of this estimated damage from the actual damage is 3.3 cm. When the level of the stochastic uncertainty is 5% and the model uncertainty is 10%, the estimated damage is at (17.5, 9.7) cm. The deviation of this estimated damage and the actual damage is 2.5 cm. By comparing the above results we can notice that the stochastic uncertainty has a higher influence on the damage localization than the model uncertainty. This is due to the fact that when the level of the stochastic uncertainty is higher than the model uncertainty, the difference between the estimated damage location and the actual damage location is higher as well as the standard deviation. As mentioned in the previous analysis, when the standard deviation increases, the confidence level decreases. The same conclusion can be drawn from the (20% stochastic uncertainty, 10% model uncertainty) and the (10% stochastic uncertainty, 20% model uncertainty).

For all the cases that the level of uncertainty is less than 20%, the difference between the estimated damage location with different levels of uncertainty and the actual damage

location is still acceptable compared to the dimensions of the plate. Engineering judgments is needed to draw conclusions if the difference is acceptable or not for the 20% case.

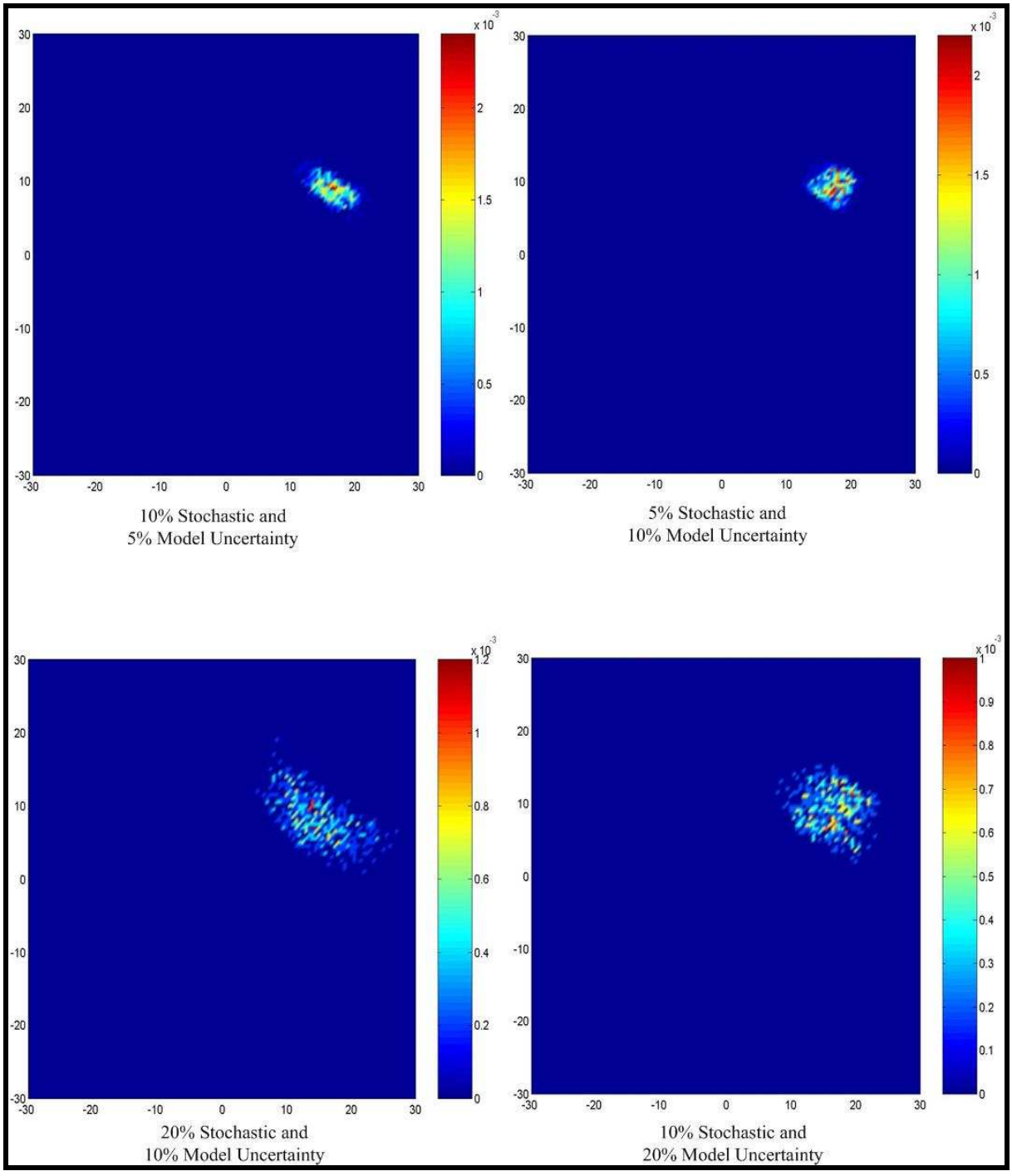

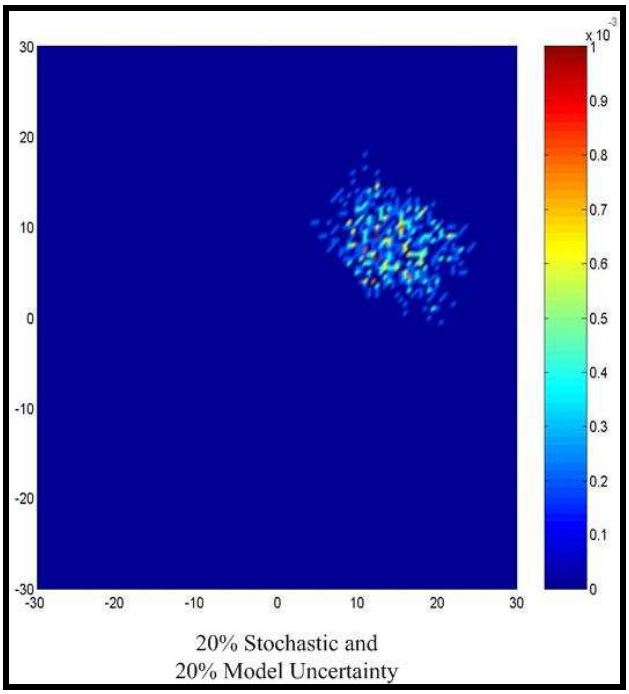

Figure 3.9 Simulation Results: Probability distribution of the damage location with different levels of stochastic and model uncertainty

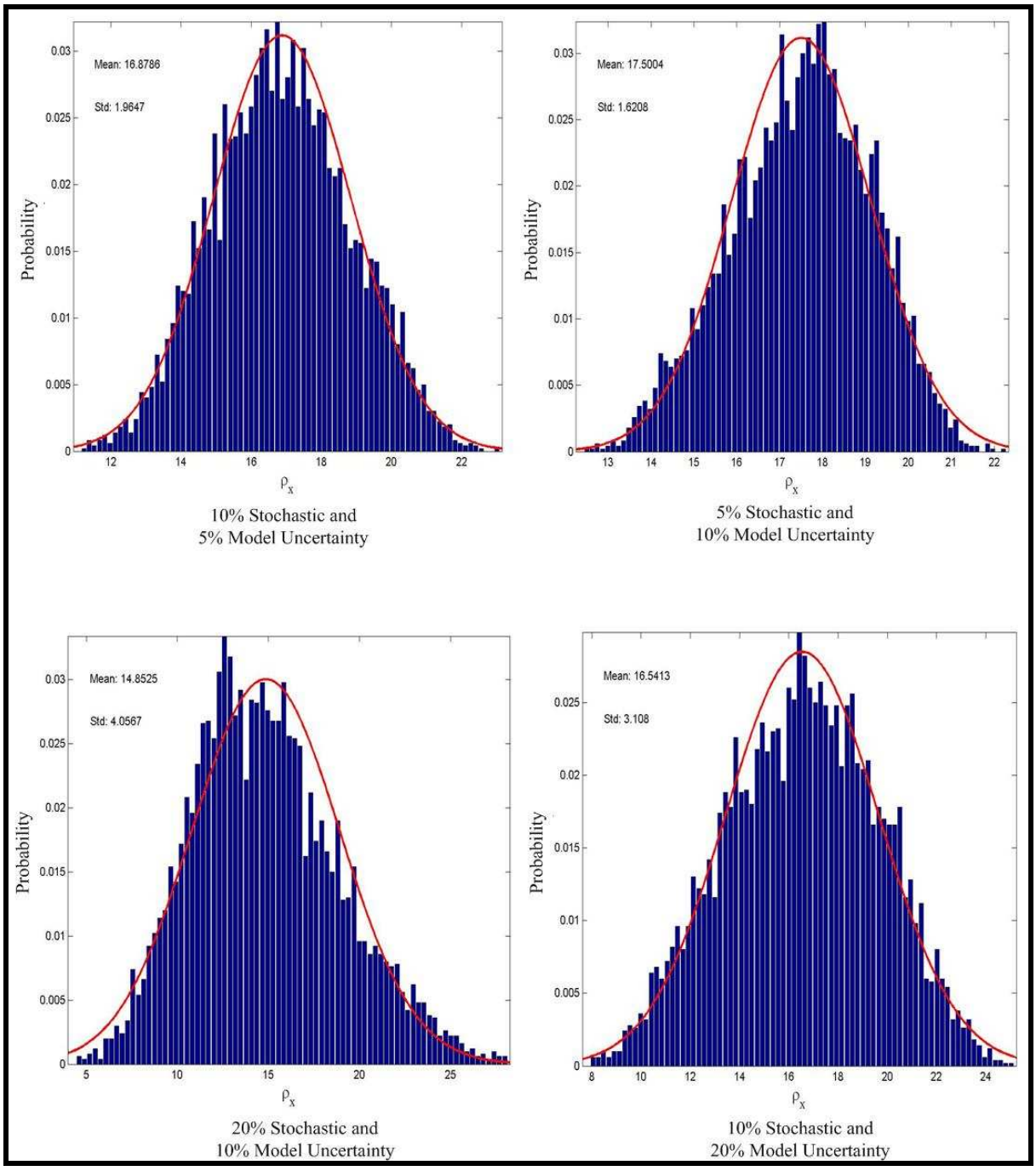
Mean: 16.8786
Std: 1.9647
Probability
ρ_x
10% Stochastic and
5% Model Uncertainty
Mean: 17.5004
Std: 1.6208
Probability
ρ_x
5% Stochastic and
10% Model Uncertainty
Mean: 14.8525
Std: 4.0567
Probability
ρ_x
20% Stochastic and
10% Model Uncertainty
Mean: 16.5413
Std: 3.108
Probability
ρ_x
10% Stochastic and
20% Model Uncertainty

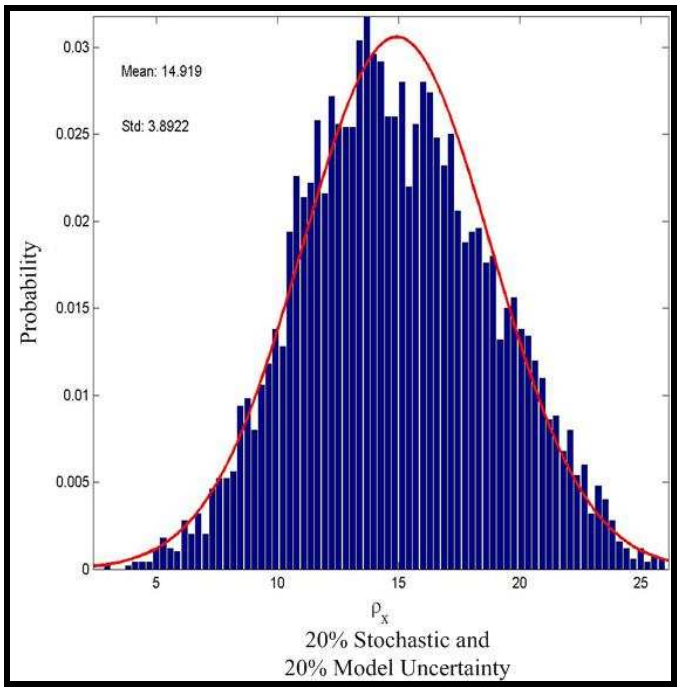

Figure 3.10 Simulation Results: Histograms and the Gaussian probability density functions of ρ_x with different levels of stochastic and model uncertainty

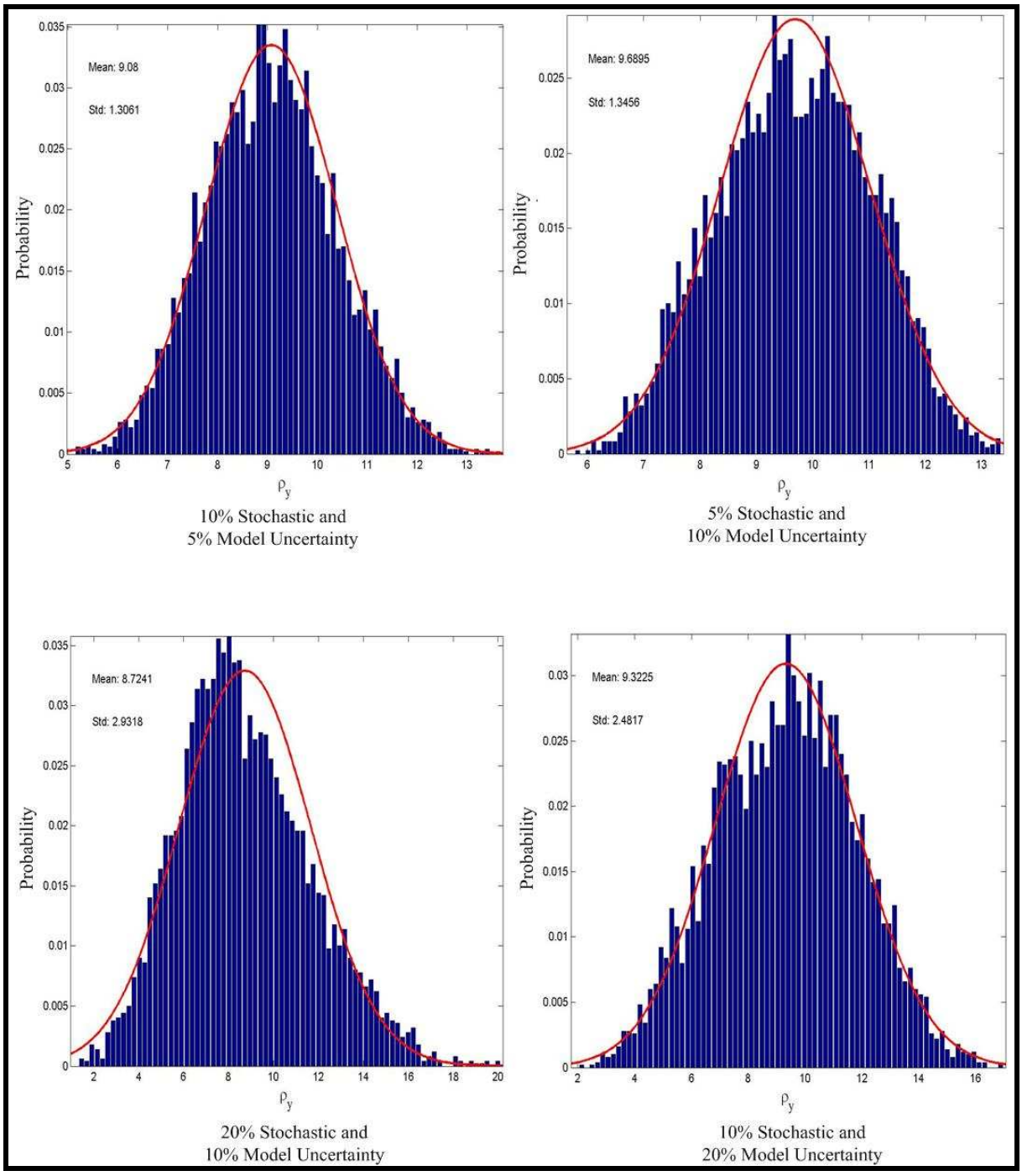
Mean: 9.08
Std: 1.3061
Probability
ρ_y
10% Stochastic and
5% Model Uncertainty
Mean: 9.6895
Std: 1.3456
Probability
ρ_y
5% Stochastic and
10% Model Uncertainty
Mean: 8.7241
Std: 2.9318
Probability
ρ_y
20% Stochastic and
10% Model Uncertainty
Mean: 9.3225
Std: 2.4817
Probability
ρ_y
10% Stochastic and
20% Model Uncertainty

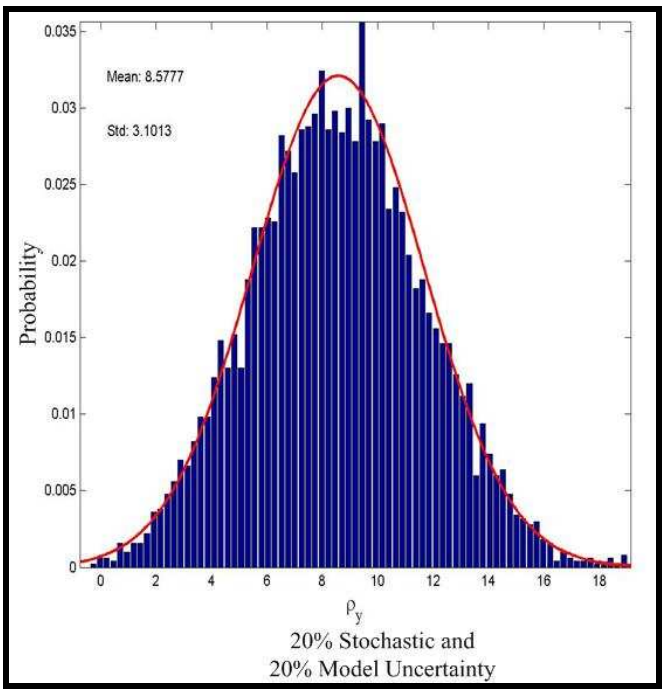

Figure 3.11 Simulation Results: Histograms and the Gaussian probability density functions of ρ_y with different levels of stochastic and model uncertainty

3.2 Experimental setup

In this section, the probabilistic approach and the least-squares method is performed on measured voltage signals to validate its capability of damage localization and studying the sensitivity of damage localization on the model and stochastic uncertainty. An aluminum plate Al-6061 with dimension $91\times91\times0.32cm^3$ is prepared and two circular rare-earth magnet stones with diameter 1.2cm are put on both sides of the plate at (-10, -10) cm to simulate a damaged area. The material properties and the geometry of the plate are listed in Table 3.4.

E (GPa)	ν	ρ (kg/m^3)	h (cm)	Dimension (cm×cm)
72.0	0.3	2730	0.32	91×91

Table 3.4 Material properties and geometry of Al-6061 plate (Experiment)

A pair of PZT disks (Navy Type II PKI502) are mounted on upper and lower sides at the central point of the plate to act as an actuator and the other four pieces of PZT disks are bonded near the four corners of the plate. Note that the diameter of PZT sensor is 6.4mm and the thickness is 1.57mm. The experimental setup as shown in Figure 3.12 consists of a HP 33120A function generator, a Tektronix TDS 420A digital oscilloscope, and a computer connected through a GPIB interface. The HP 3220A function generator is used to generate a 50 KHz five-peaked signal. The signal is sent to TDS420A oscilloscope and K-H7602 amplifier. The sampling rate of TDS420A is set as 500kHz. The peak voltage of the excitation signal from the amplifier is kept at ±50V, which translates into an electric field intensity of about 31.25V/mm, below the maximum operating field of 300V/mm. Then the response signals measured by sensors are displayed and stored in the digital oscilloscope. Finally, the computer obtains the collected date via GPIB interface and runs the probabilistic

approach and the least-squares algorithm to estimate the damage location. Figure 3.13 shows the reflected wave signals from damage received by the four sensors.

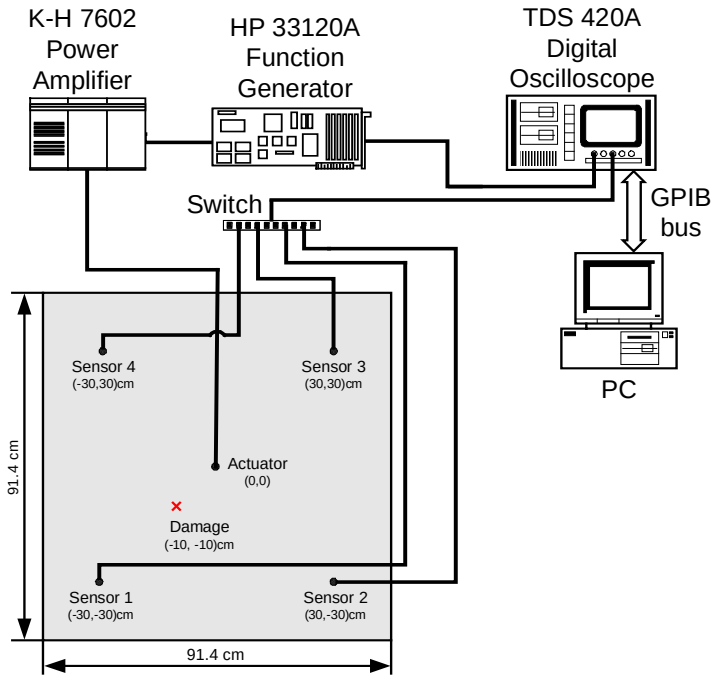

Figure 3.12 Experimental Setup for Damage Localization

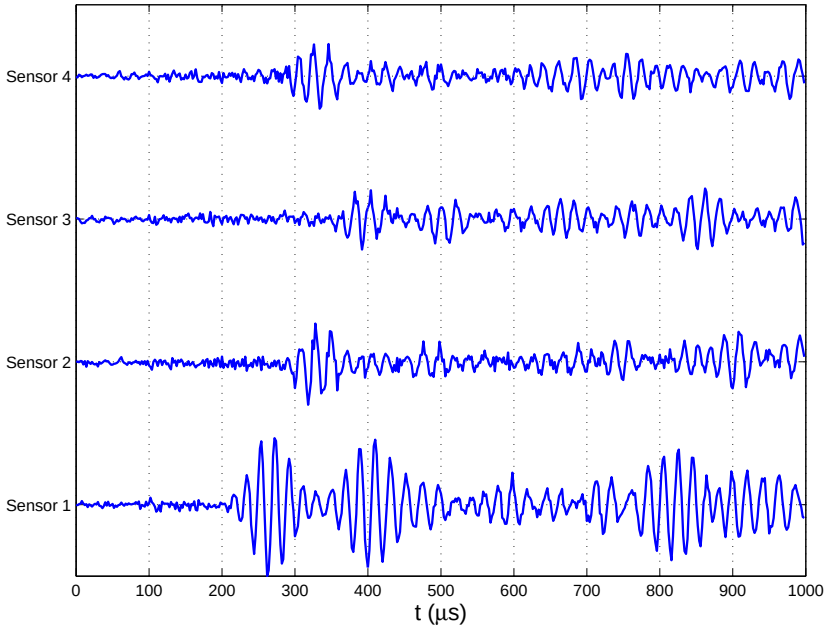

Figure 3.13 The reflected wave signal received by each sensor

3.3 Experimental Results and Discussion

To validate the simulation results, the same analysis is preformed on experimental data (Wang, 2004). Figures 3.14 and 3.15 show the plots of the different searching traces (three traces in each figure) with different initial guesses with zero level of uncertainty. The targeted damage location is (-10, -10) cm. The method converges to a damage position (-10, -8.8) cm, which makes the error between the actual damage location and the estimated damage location to be 1.2 cm. From this result, it can be seen that this method has a robust performance and is validated through experimental results.

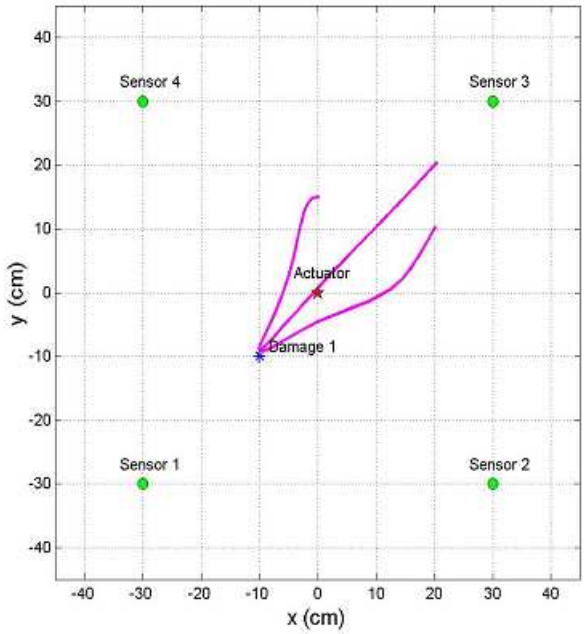

Figure 3.14 Experimental results of damage localization by least-squares method

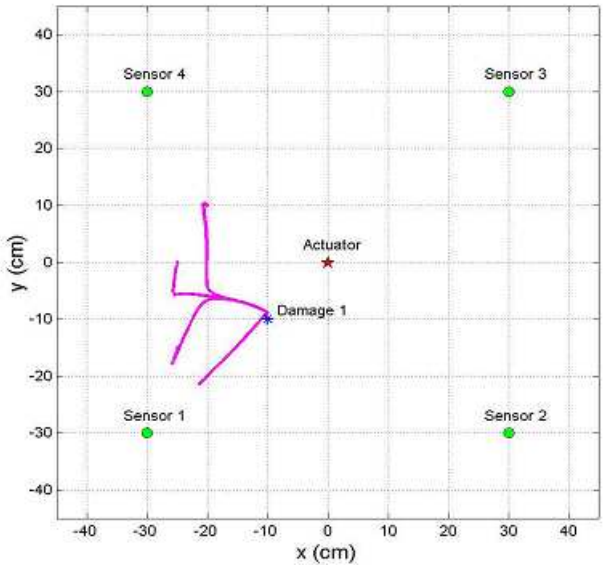

Figure 3.15 Experimental results of damage localization by least-squares method

The test was performed in the controlled laboratory environment, to accommodate the field environment. Figures 3.16, 3.17 and 3.18 show the probability distribution, the histograms and the PDFs for different levels of stochastic uncertainty. The estimated damage with 5% stochastic is at (-8.8, -8.4) cm. The estimated damage location with 10% stochastic uncertainty and 20% stochastic uncertainty is at (-8.3, -7.9) cm and (-7.6, -7.1) cm, respectively. From the PDFs, one can conclude that when the level of the stochastic uncertainty changes, the mean and the standard deviation of the PDFs change. Similar to the simulation results, the stochastic uncertainty has an influence both on the mean and the standard deviation. Also, from the results, one can deduce that as the level of stochastic uncertainty increases, the estimated damage location deviates from the actual damage location.

Table 3.4 summarizes the different level of stochastic uncertainties that has been used in the experimental analysis as well as the results that make good agreement with the simulation

results. Table 3.5 shows the difference between the estimated damage location with different levels of uncertainty and the actual damage location.

	Stochastic Uncertainty	Estimated Damage Location (cm)	Standard Deviation (σ_x, σ_y) (cm)	Difference (cm) between the estimated damage and the actual damage location (-10, -10) cm
Level of Uncertainty	5%	(-8.9, -8.5)	(0.6, 0.6)	2.0
	10%	(-8.4, -8.0)	(1.2, 1.2)	2.7
	20%	(-7.6, -7.1)	(2.2, 2.1)	3.7

Table 3.5 Influences of the level of stochastic uncertainty on Damage Localization (Experimental Results)

For all the different levels of the stochastic uncertainty (5%, 10%), the difference between the estimated damage with 5%, 10% uncertainty and the actual damage location is low. Therefore, the results are very acceptable compared to the dimensions of the plate $91\times91\times0.32cm^3$. For 20% stochastic uncertainty, engineering judgment is needed to draw conclusions about the results.

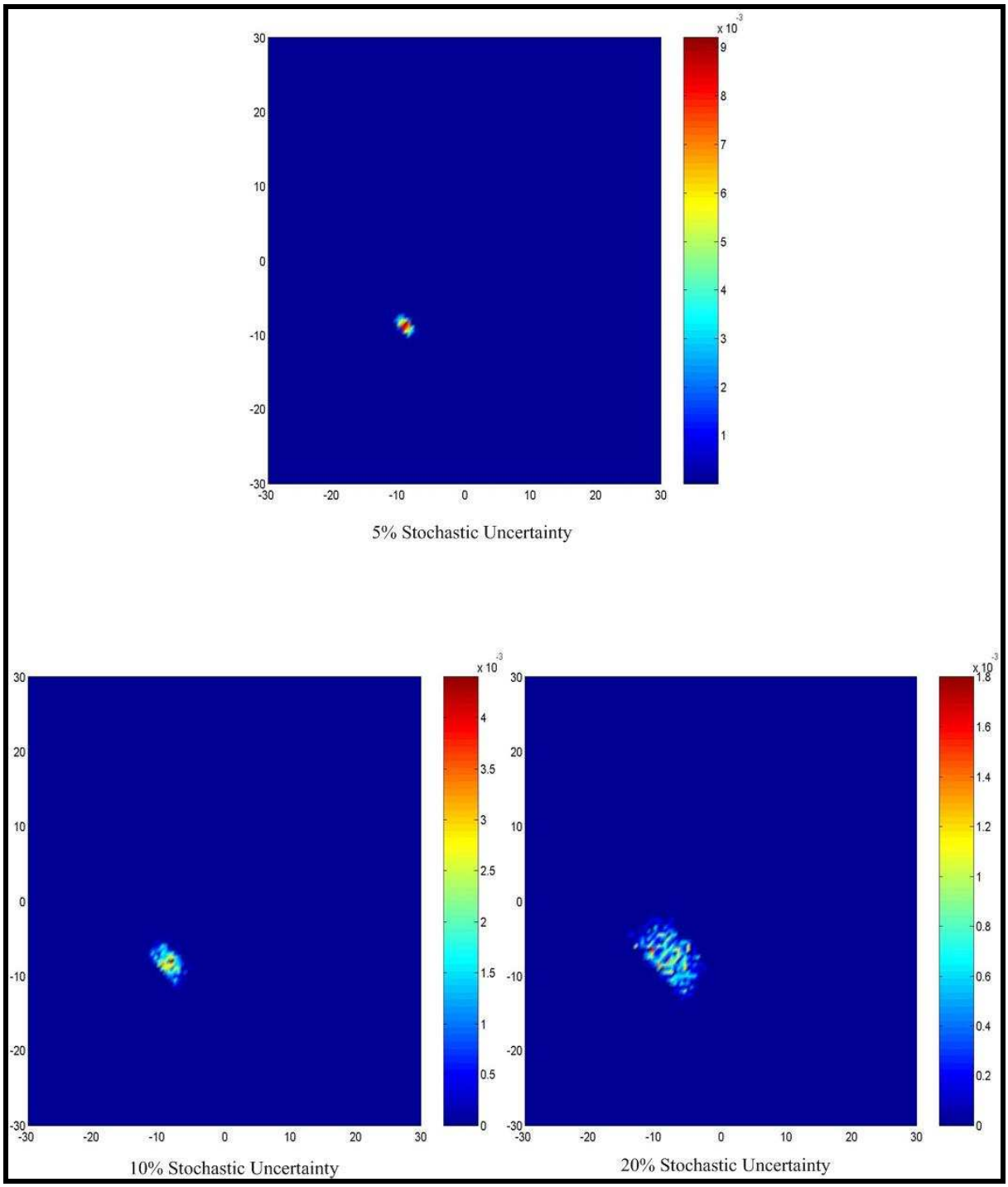

Figure 3.16 Probability distribution of the damage location with different levels of stochastic uncertainty

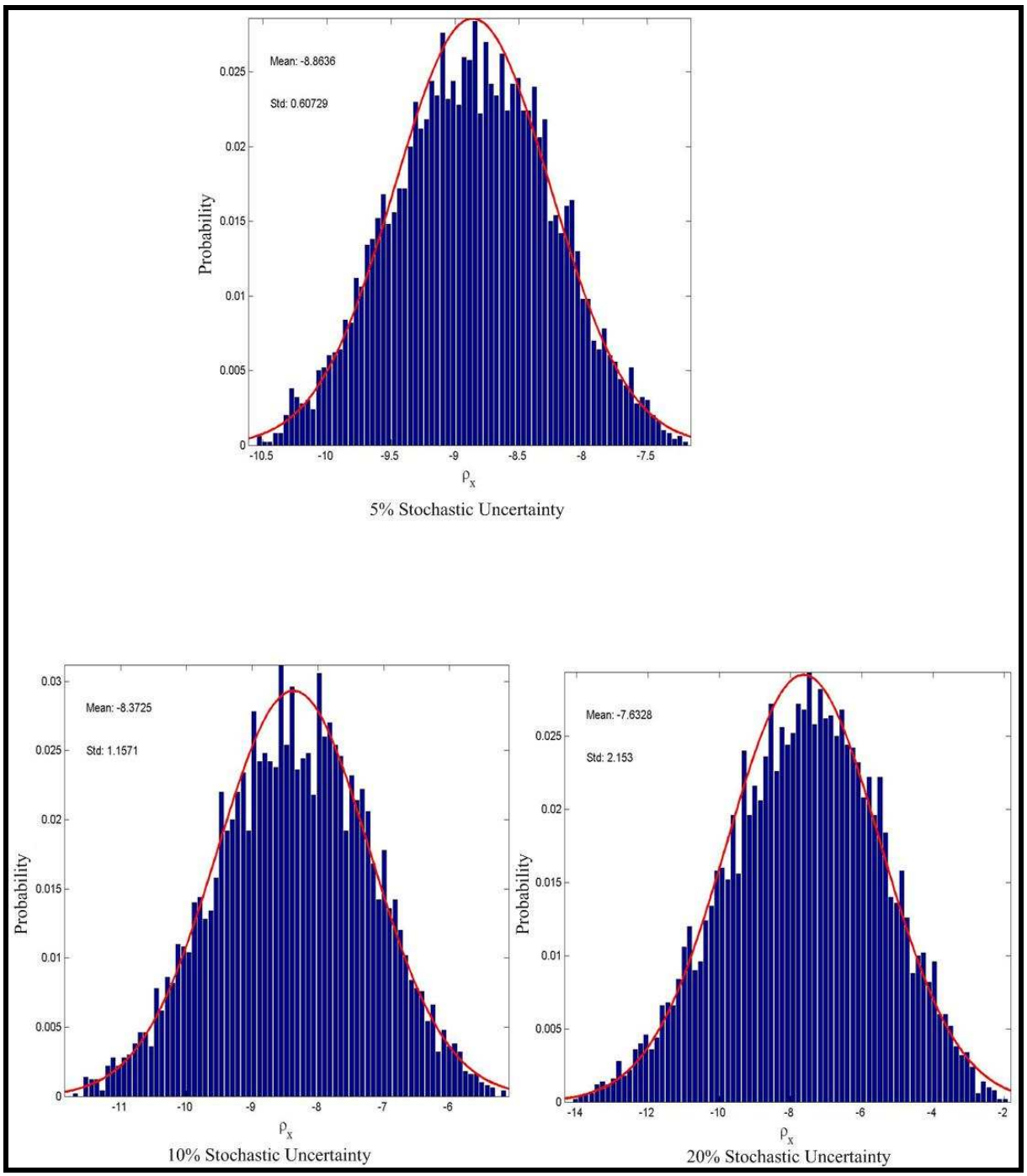

Figure 3.17 Histograms and the Gaussian probability density functions of ρ_x with different levels of stochastic uncertainty

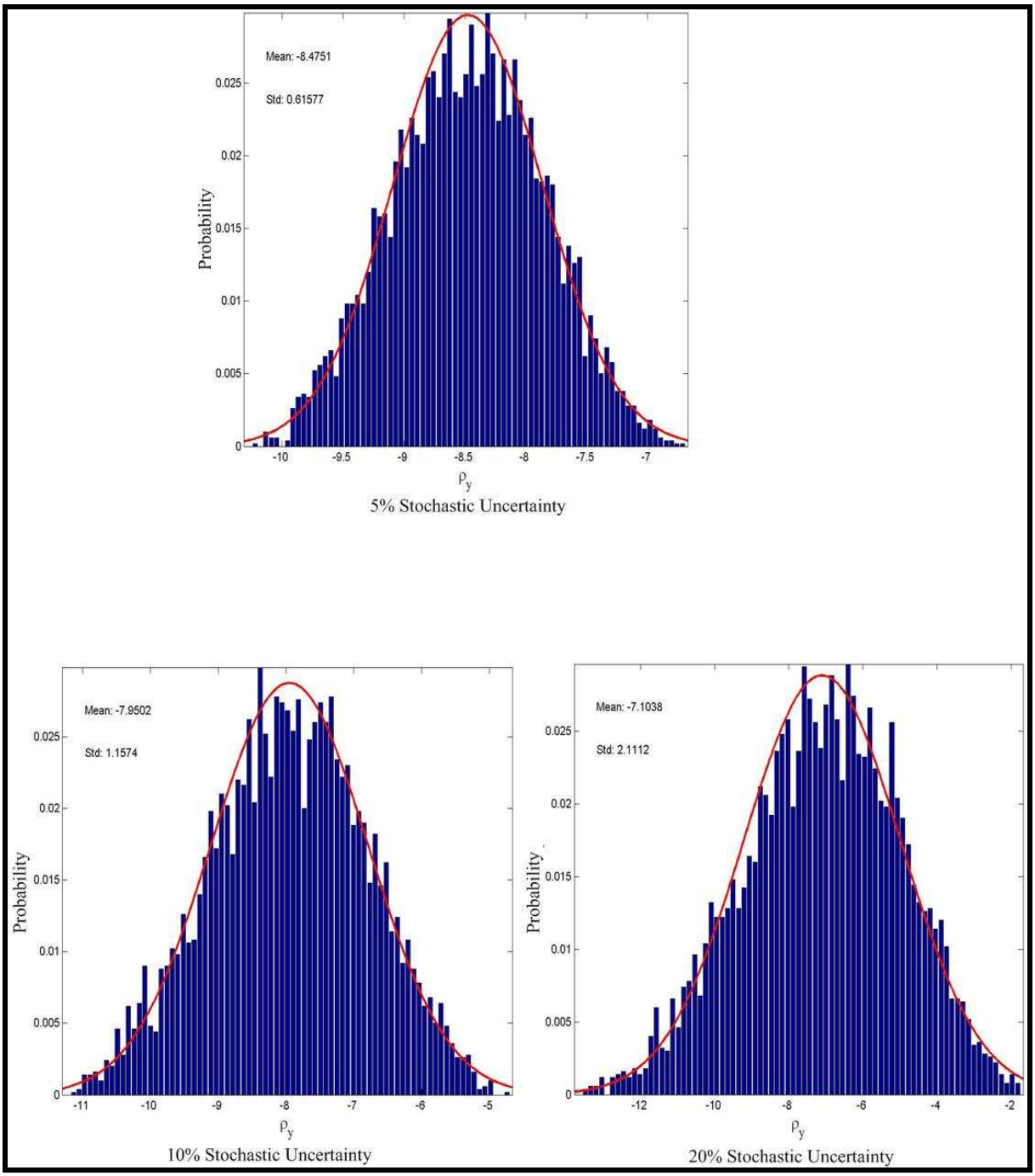

Figure 3.18 Histograms and the Gaussian probability density functions of ρ_y with the different levels of stochastic uncertainty

To validate the simulation results, the analysis of having 5%, 10% and 20% stochastic and model uncertainties at the same time has been studied again using the experimental data. Also, this analysis has been done to prove the conclusion that has been drawn previously, which states that the damage localization is more sensitive to the stochastic uncertainty rather than the model uncertainty. Table 3.6 presents the different levels of stochastic and model uncertainty and the corresponding results.

	Stochastic Uncertainty	Model Uncertainty	Estimated Damage Location (cm)	Standard Deviation (σ_x, σ_y) (cm)	Difference (cm) between the estimated damage and the actual damage location (-10, -10) cm
Level of Uncertainty	10%	5%	(-8.8, -7.9)	(1.8, 1.7)	2.4
	5%	10%	(-9.0, -8.6)	(1.9, 1.9)	1.8
	20%	10%	(-7.7, -7.1)	(2.9, 2.8)	3.7
	10%	20%	(-9.0, -8.0)	(3.6, 3.5)	2.2
	20%	20%	(-7.7, -7.3)	(3.9, 3.8)	3.5

Table 3.6 Influence of the interaction of two different kinds of uncertainty (Experimental Results)

Figure 3.19 through Figure 3.21 show the probability distribution, the histograms and the PDFs for different levels of stochastic and model uncertainty. When the level of stochastic uncertainty is 10% and the model uncertainty is 5%, the estimated damage is at (-8.8, -7.9) cm. The deviation of this estimated damage from the actual damage is 2.4 cm. When the level of the stochastic uncertainty is 5% and the model uncertainty is 10%, the estimated damage is at (-9.0, -8.6) cm. The difference between this estimated damage and the actual damage is 1.8 cm. By comparing the above results we can notice that the stochastic uncertainty has a higher influence on the damage localization than the model uncertainty. This is due to the fact that when the level of the stochastic uncertainty is higher than the model uncertainty, the difference between the estimated damage location and the actual damage location is higher as well as the standard deviation. As mentioned in the previous

analysis, when the standard deviation increases, the confidence level decreases. The same conclusion can be drawn from the (20% stochastic uncertainty, 10% model uncertainty) and the (10% stochastic uncertainty, 20% model uncertainty).

For all the cases that the level of uncertainty is less than 20%, the difference between the estimated damage location with uncertainty and the actual damage is less than 3 cm. Compared to the dimensions of the plate, the results are acceptable. Engineering judgments is needed to draw conclusions if the difference is acceptable or not for the 20% case. Therefore, the simulation results are valid because the experimental results matched the simulation results very well. Note that the damage shape was circular with a diameter equal to 1.2 cm. So, the estimated damage in here does not correspond to the center of the actual circular damage. It corresponds to the edges of the circle because the measured signals are reflected from the edges of the damage.

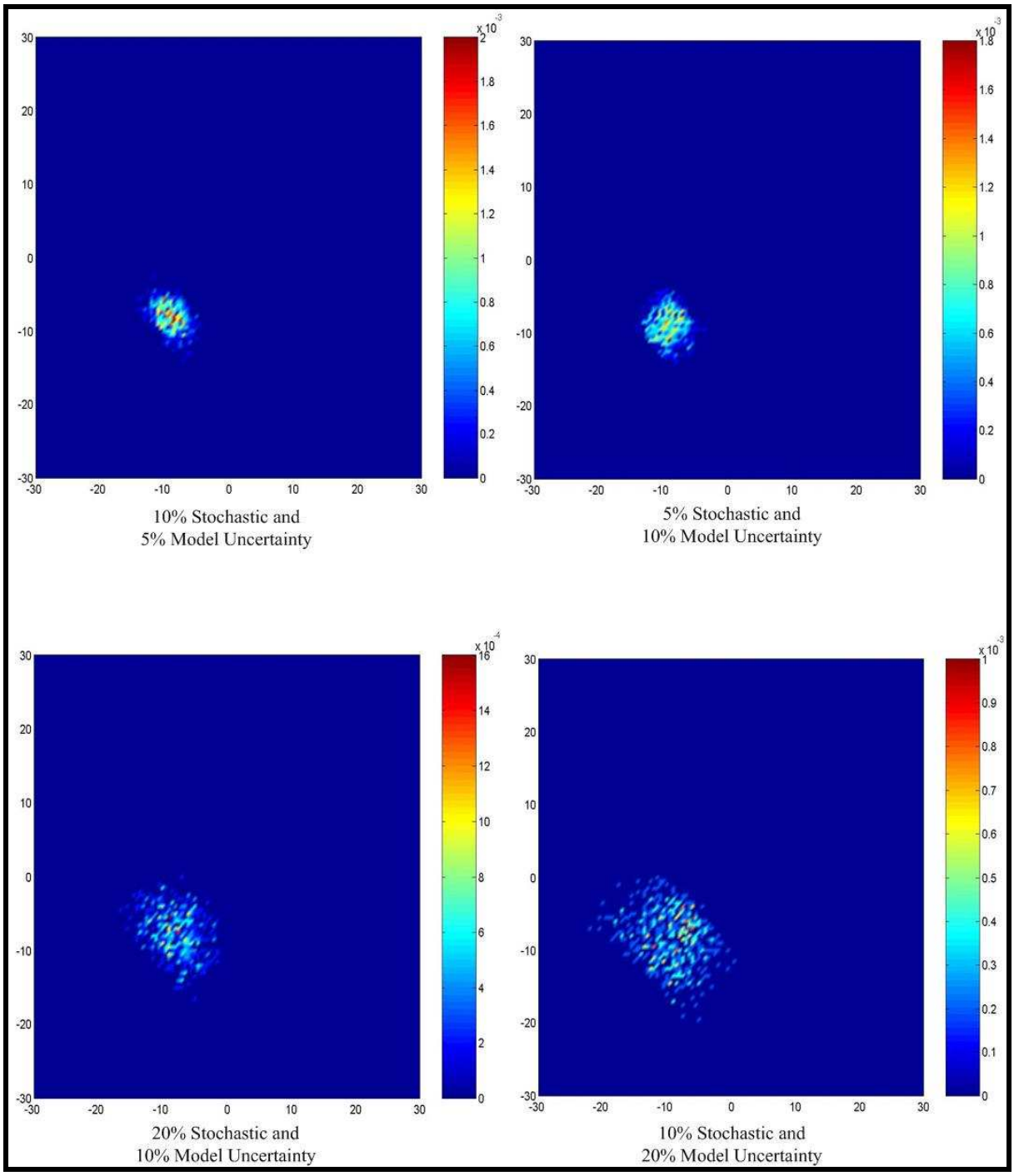
10% Stochastic and
5% Model Uncertainty
5% Stochastic and
10% Model Uncertainty
20% Stochastic and
10% Model Uncertainty
10% Stochastic and
20% Model Uncertainty

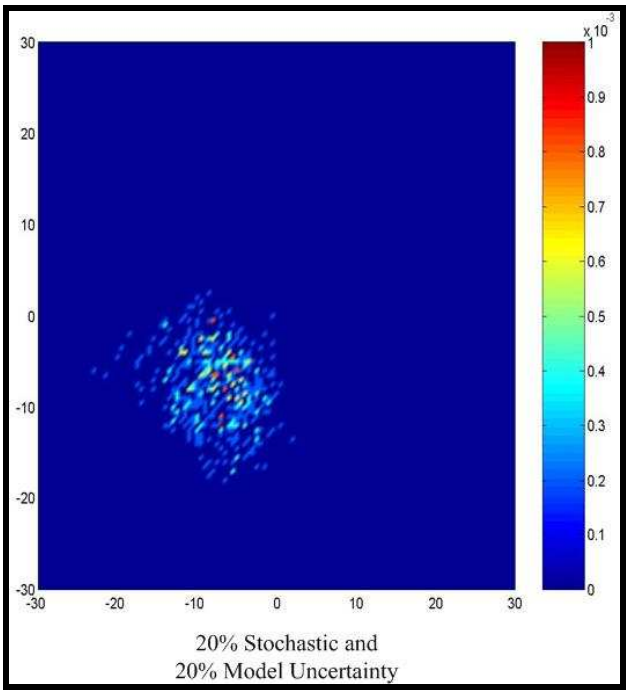

Figure 3.19 Probability distribution of the damage location with different levels of stochastic and model uncertainty

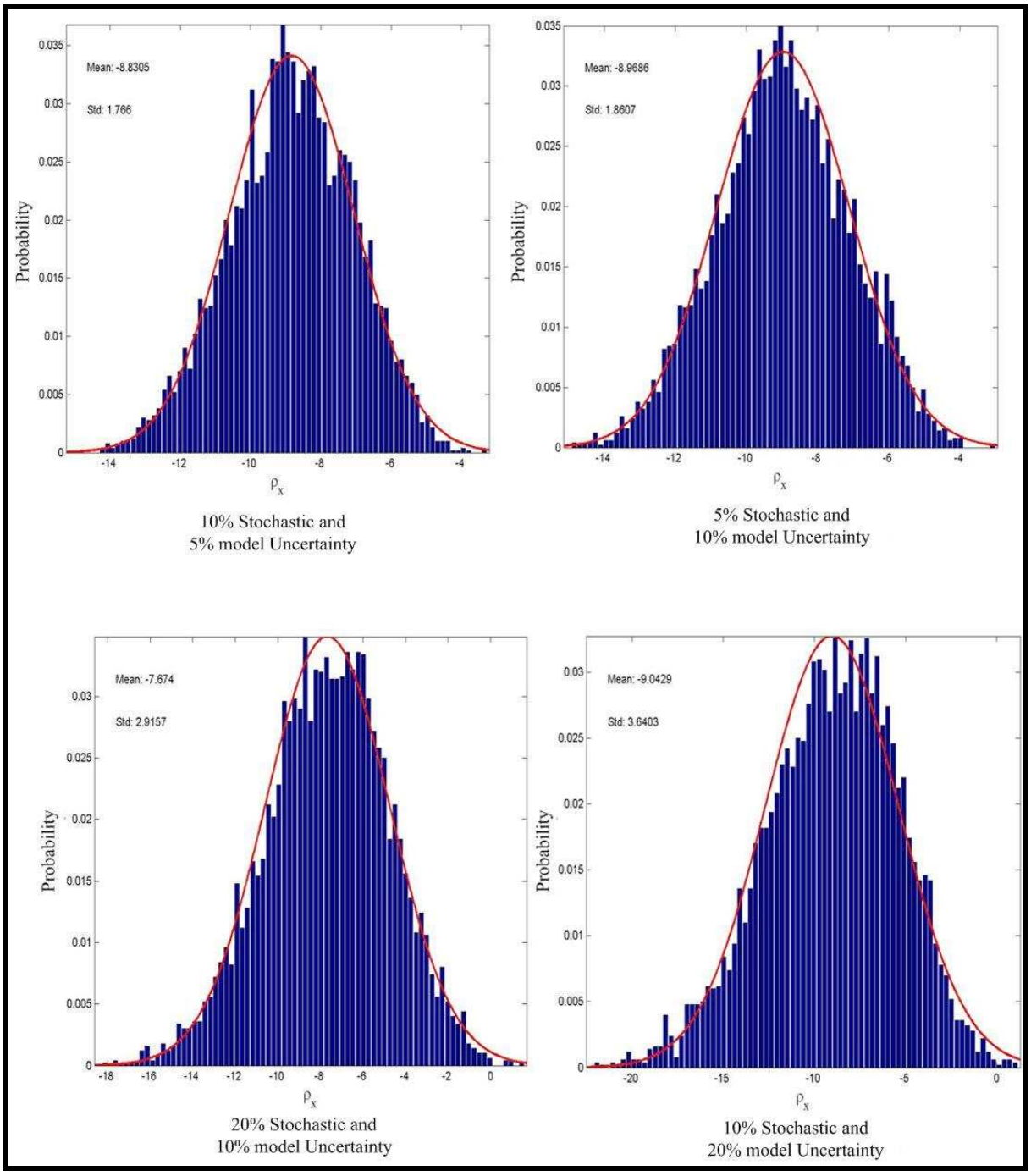
Mean: -8.8305
Std: 1.766
Probability
ρ_x
10% Stochastic and
5% model Uncertainty
Mean: -8.9686
Std: 1.8607
Probability
ρ_x
5% Stochastic and
10% model Uncertainty
Mean: -7.674
Std: 2.9157
Probability
ρ_x
20% Stochastic and
10% model Uncertainty
Mean: -9.0429
Std: 3.6403
Probability
ρ_x
10% Stochastic and
20% model Uncertainty

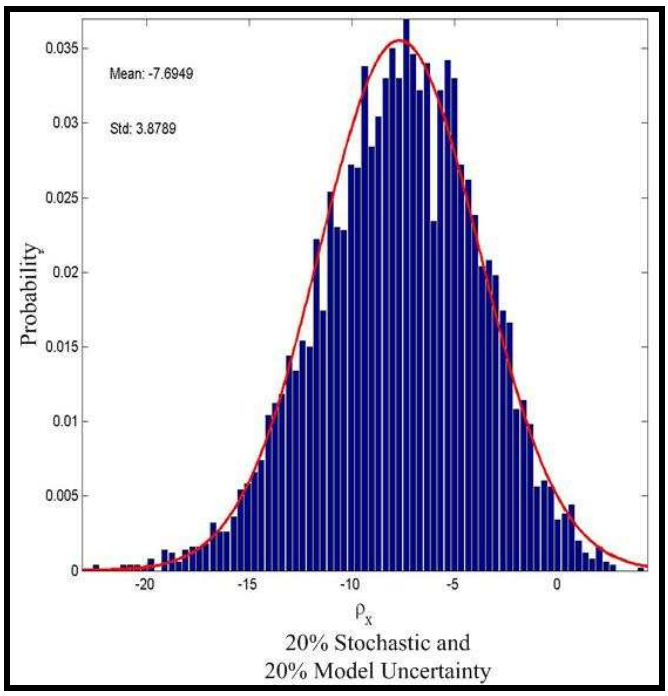

Figure 3.20 Histograms and the Gaussian probability density functions of ρ_x with different levels of stochastic and model uncertainty

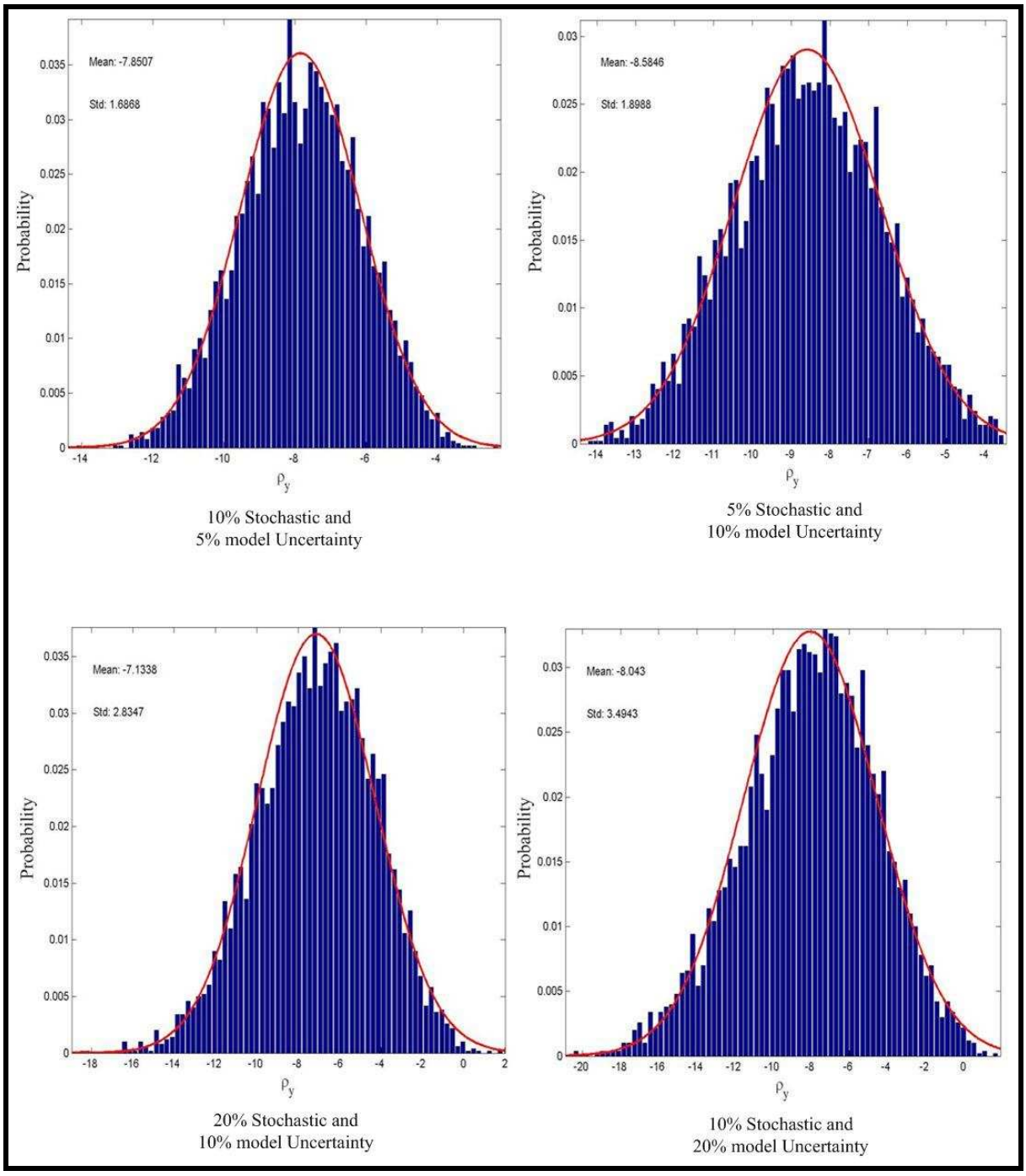

10% Stochastic and
5% model Uncertainty

5% Stochastic and
10% model Uncertainty

20% Stochastic and
10% model Uncertainty

10% Stochastic and
20% model Uncertainty

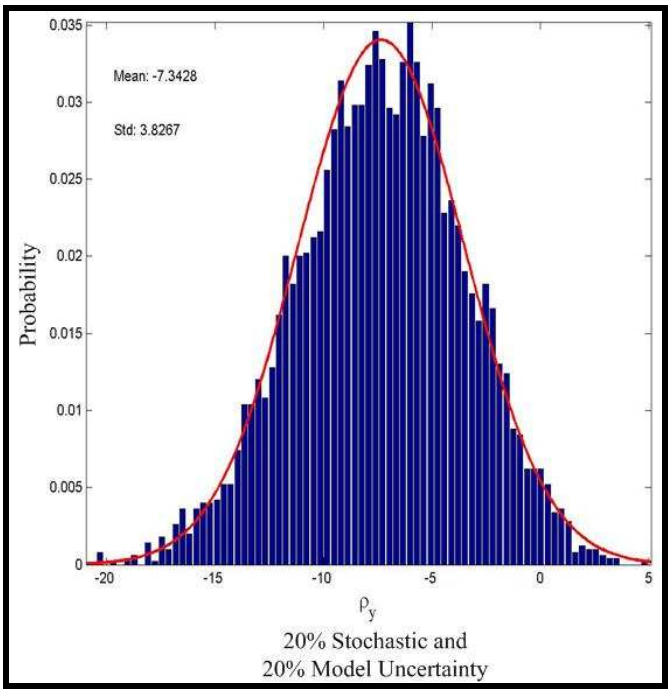

Figure 3.21 Histograms and the Gaussian probability density functions of ρ_y with different levels of stochastic and model uncertainty

4 Conclusions

The ultimate objective of establishing Structural Health Monitoring (SHM) system is to continuously monitor and assess the status of the integrity of a structure or its components with a high level of confidence and reliability. In general, the common techniques employed in SHM for monitoring structures and detecting damages can be divided into two categories: (1) vibration-based approach and (2) wave-based approach. Since wave-based approach can provide better local health status information and has higher sensitivity to damages than vibration-based approach, this thesis focuses on damage localization of plate structure using wave-based approach.

The need for structural health monitoring that takes into account the stochastic and model uncertainty in the problem and lends itself well to in-situation application motivates this work. The method presented in this work originates from the wave-based approach and considers the uncertainty effects aiming at answering the following question in a probabilistic method:

Based on the sensor data, and acknowledging the uncertainty in the problem, what is the probability that the damage occurs at a certain location in a structure?

In order to answer the above question, probabilistic descriptions for different types of uncertainties are needed. The Monte Carlo simulation is capable of generating random numbers from a Gaussian distribution. The Monte Carlo method is used to model the probability density function for each uncertainty or interaction of uncertainties. Finally the resulting PDF of the damage location is obtained. For each sample generated from the Monte

Carlo simulation, a least-squares method is applied to iteratively search for the damage location based on elastic wave energy measurements.

Based on the efforts described in this work, a number of conclusions can be drawn:

- A framework that accounts for uncertainty for the damage localization in a structured fashion is successfully developed.

- The Monte Carlo simulation is very suitable for modeling uncertainties when dealing with statistical analysis. The Monte Carlo simulation appears to be the only universal method that can provide accurate solutions for many problems. The major advantage of the Monte Carlo simulation is that accurate solutions can be obtained for any problem whose deterministic solution is known. The only disadvantage of the Monte Carlo simulation is that it is generally time consuming. Other methods such as the Latin Hypercube, which are more computationally efficient, may be used.

- The probabilistic approach is capable of showing the effect of the level of uncertainties on the damage localization. The results show that the damage localization is more sensitive to the stochastic uncertainty than the model uncertainty. This implies that the elastic wave energy decay model is accurate and robust.

- The key aspect of the probabilistic approach is the minimization of false-positive and false-negative indicators from the damage localization process. False- positive refers to the situation where damage is indicated when in fact

none is present. False- negative refers to the situation where damage is not indicated, even though it is present. The false alarm can be minimized by analyzing the probability distributions of the damage location.

- The method is an active damage detection technique, which is suitable for the applications of SHM.

- The method uses the all time series data information collected by each sensor not only the time-of-flight or time of arrival. From the experimental and simulation results, it was shown that the estimated damage location by least-squares method makes good agreement with the targeted location.

5 References

[1] Augusti, G., Baratta, A., and Casciati, F. (1984), *Probabilistic Methods in Structural Engineering*, Chapman and Hall, London.

[2] Ayyub, B. M. and Gupta, M. M. (1994), *Uncertainty Modeling and Analysis: Theory and Applications*, Elsevier Science, Amsterdam, The Netherlands.

[3] Baruh, H. and Ratan, S. (1993), "Damage Detection in Flexible Structures", *Journal of Sound and Vibration*, Vol. 166, pp. 21-30.

[4] Beck, J. L. and Au, S. K. (2001), "Monitoring Structural Health Using a Probabilistic Measure", *Computer-Aided Civil and Infrastructure Engineering*, Vol. 16, pp. 1-11.

[5] Beck, J. L. (1996), "System Identification Methods Applied to Measured Seismic Response", *Proceedings of the Eleventh World Conference on Earthquake Engineering*, Acapulco, Mexico.

[6] Caughey, T. K. and O'Kelly, M. E. J. (1965), "Classical Normal Modes in Damped Linear Dynamic System", *Journal of Applied Mechanics*, Vol. 32, Issue 3, pp. 89-95.

[7] Chang, F. K. (1999), "Structural Health Monitoring, a Summary Report on the first International Workshop on Structural Health Monitoring", *The 2nd International Workshop on Structural Health Monitoring*, Stanford University, pp. xix-xxix.

[8] Devore, J. L. (1987), *Probability and Statistics for Engineering and the Sciences*, Wadsworth, Belmont, California.

[9] Dornheim, M. A. (2004), "Hidden Fatigue Cracks Suspected in C-130 Crash", *Aviation Week and Space Technology*, http://www.aviationnow.com/content/publication/awst/20020902/aw48.htm.

[10] Doebling, S. W. and Farrar, C. R. (1998), "Statistical Damage Identification Techniques Applied To the I-40 Bridge Over The Rio Grande River", *Proceedings of 16th International Modal Analysis Conference*, Santa Barbara, CA, pp. 1717-1724.

[11] Faragher, J. (2004), "Probabilistic Methods for the Quantification of Uncertainty and Error in Computational Fluid Dynamics Simulations", DSTO-TR-1633.

[12] Fugate, M. L., Sohn, H., and Farrar, C. R. (2000), "Unsupervised Learning Methods for Vibration-Based Damage Detection" *Presented at IMAC 18*, San Antonio, Texas.

[13] Fugate, M. L., Sohn, H., and Farrar, C. R. (2001), "Vibration-Based Damage Detection Using Statistical Process Control", *Mechanical Systems and Signal Processing,* Vol. 15, No. 4, pp. 707-721.

[14] Jaynes, E. T. (1978), Where Do We Stand on Maximum Entropy?, *The maximum Entropy Formalism*, MIT Press, Cambridge, MA.

[15] Katafygiotis, L. S., Lam, H. F., and Mickleborough, N.C. (2000), "Application of A Statistical Approach on a Benchmark Damage Detection Problem", *EM2000 Fourteenth Engineering Mechanics Conference*, Austin Texas.

[16] Kim, J. T. and Stubbs, N. (1995), " Model-Uncertainty Impact and Damage-Detection Accuracy in Plate Grider", *Journal of Structural Engineering*, Vol. 121, No. 10, pp. 1409-1417.

[17] Lannotta, B. (2004), "Safe Launches for CEV", *Aerospace America*, pp. 40-44.

[18] Lin, X. and Yuan, F. G. (2001), "Damage Detection of a Plate Using Migration Technique", *Journal of Intelligent Material Systems and Structures*, Vol. 12, No. 3, pp. 469-482.

[19] Moller, B. and Beer, M. (2004), *Fuzzy Randomness: Uncertainty in Civil Engineering and Computational Mechanics*, Springer-Verlag, Berlin, Germany.

[20] Nowak, A. S. and Collins, K. R. (2000), *Reliability of Structures*, The McGraw-Hill Companies, USA.

[21] Shapiro, J. (2003), "Probability and Bayesian Classification", www.cs .man.ac.uk/ ~jls/CS2411/probability.pdf.

[22] Siddall, J. N. (1983), *Probabilistic Engineering Design, Principles and Applications*, Marcel Dekker Inc., New York and Basel.

[23] Sohn, H., Farrar, C. R., Hunter, F. N., and Worden, K. (2001), "Structural Health Monitoring Using Statistical Pattern Recognition Techniques", *Journal of Dynamic Systems, Measurement, and Control*, Vol. 123, pp. 706-711.

[24] Sohn, H., Park, G., Wait, J. R., Limback, N. P., and Farrar, C. R. (2004), "Wavelet-based Active Sensing for Delamination Detection in Composite Structures", *Smart Materials and Structures*, Vol. 13, No. 1, pp. 153-160.

[25] Vanik, M. W. (1997), "A Bayesian Probabilistic Approach for Structural Damage Detection", *PhD thesis, California Institute of Technology*, Pasadena, California.

[26] Vanik, M. W., Beck, J. L., and Au, S. K. (2000), "Damage Detection Using Outlier Analysis", *Journal of Sound and Vibration*, Vol. 229, No. 3, pp. 647-667.

[27] Vanik, M. W., Beck, J. L., and Au, S. K. (2000), "Bayesian Probabilistic Approach to Structural Health Monitoring", *Journal of Engineering Mechanics*, Vol. 126, No. 7, pp. 738-745.

[28] Wang, L. (2004), "Elastic Wave Propagation in Composites and Least-Squares Damage Localization Technique", *Master's Thesis, North Carolina State University*, Raleigh, North Carolina.

[29] Weise, K. and Woger, W. (1992), "A Bayesian Theory of Measurement Uncertainty", *Measurement Science and Technology*, Vol. 4, pp. 1-11.

[30] Yang, S. and Yuan, F. G. (2005), "Transient Wave Propagation of Isotropic Plates Using a Higher-Order Plate theory", *International Journal of Solids and Structures*, Vol. 42, No. 14, pp. 4115-4153.